Journal of Medicinal Chemistry

pubs.acs.org/jmc

Article

Discovery and Characterization of a First-In-Class HCK/BTK PROTAC DFCI-002-06 for the Treatment of MYD88 Mutated B Cell Malignancies

John M. Hatcher,[⊥] Shirong Liu,[⊥] Amanda Kofides, Alexa Canning, Dominic Pizzarella, Xia Liu, Nickolas Tsakmaklis, Maria Guerrera, Christopher Patterson, Alberto Guijosa, Prafulla Gokhale, Zachary Hunter, Shayna Sarosiek, Jorge Castillo, Jinhua Wang, Sara J. Buhrlage, and Steven P. Treon*

Cite This: *J. Med. Chem.* 2026, 69, 1119−1134

Read Online

ACCESS | Metrics & More | Article Recommendations | Supporting Information

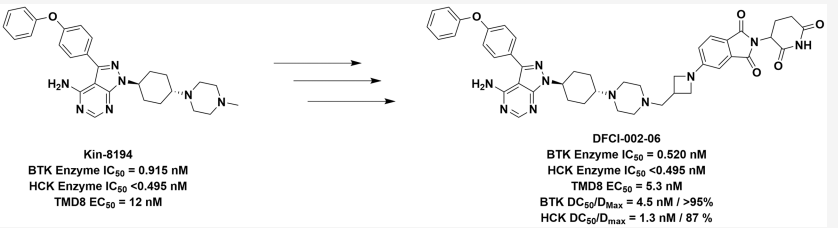

ABSTRACT: Hematopoietic cell kinase (HCK) and Bruton tyrosine kinase (BTK) are critical drivers of survival signaling in MYD88-mutated ($MYD88^{Mut}$) lymphomas. Building on our previously developed dual HCK/BTK inhibitor KIN-8194, we designed **DFCI-002-06**, a first-in-class proteolysis-targeting chimera (PROTAC) that potently and selectively degrades both kinases while retaining kinase inhibitory activity with improved selectivity versus KIN-8194. DFCI-002-06 induced enhanced apoptosis in $MYD88^{Mut}$ lymphoma cells and remained active against ibrutinib-resistant BTK^{Cys481} variants. The compound demonstrated high oral bioavailability in mice (F = 39%), favorable pharmacokinetics, and dose-dependent degradation of HCK and BTK in tumors. In TMD8 xenograft models, orally dosed **DFCI-002-06** produced superior tumor suppression and prolonged survival compared to KIN-8194. Preclinical safety studies showed a favorable profile, including a negative Ames test, no hERG inhibition at relevant concentrations, and excellent tolerability in a 21 day rat toxicity study. **DFCI-002-06** represents a rational dual-target degradation strategy for $MYD88^{Mut}$ lymphomas.

INTRODUCTION

Activating mutations in MYD88 ($MYD88^{Mut}$) are highly recurrent across a spectrum of B cell malignancies, including Waldenström's macroglobulinemia (WM; 95−97%), primary CNS lymphoma (PCNSL; 70−80%), the ABC subtype of diffuse large B cell lymphoma (ABC-DLBCL; 30−40%), marginal zone lymphoma (MZL; ∼10%), and chronic lymphocytic leukemia (CLL; 8−15%).[1−6] $MYD88^{Mut}$ initiate pro-survival signaling cascade via assembly of the Myddosome, a protein complex that activates BTK and other pathways.[7−11] Based on these findings, we and others developed covalent and noncovalent BTK inhibitors for WM and other B cell malignancies. In WM, BTK inhibitors exhibit the highest level for single drug therapeutic activity.[12] Both ibrutinib and zanubrutinib are approved for the treatment of symptomatic WM. Despite their clinical success, both intrinsic and acquired resistance limit the clinical activity of BTK inhibitors. Acquired mutations at BTK^{Cys481} interfere with the binding of covalent and noncovalent BTK inhibitors, resulting in loss of efficacy and restoration of downstream signaling.[12,13] Moreover, treatment with BTK inhibitors rarely induces complete responses, suggesting that additional upstream signaling in the MYD88 pathway sustain pro-survival signaling (see Table 1, Scheme 1).

Hematopoietic cell kinase (HCK) is a SRC family member that is normally downregulated in late-stage B cell development.[14] HCK is highly expressed in WM, and its expression is transcriptionally upregulated by $MYD88^{Mut}$ as well as activated by $MYD88^{Mut}$ via IL-6/JAK2/STAT3 signaling.[8,9,15] Activated HCK triggers BTK mediated NF-κB signaling and also drives parallel activation of ERK1/2, AKT, and SYK thereby establishing HCK as a central mediator of $MYD88^{Mut}$ pro-survival signaling (Figure 1).[8−11] $MYD88^{Mut}$ driven HCK activity has also been implicated in mediating paracrine resistance to BTK inhibitors via ERK1/2 driven cytokine release in the tumor microenvironment.[9] The noncovalent BTK

Received: August 27, 2025
Revised: December 12, 2025
Accepted: December 16, 2025
Published: January 3, 2026

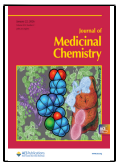

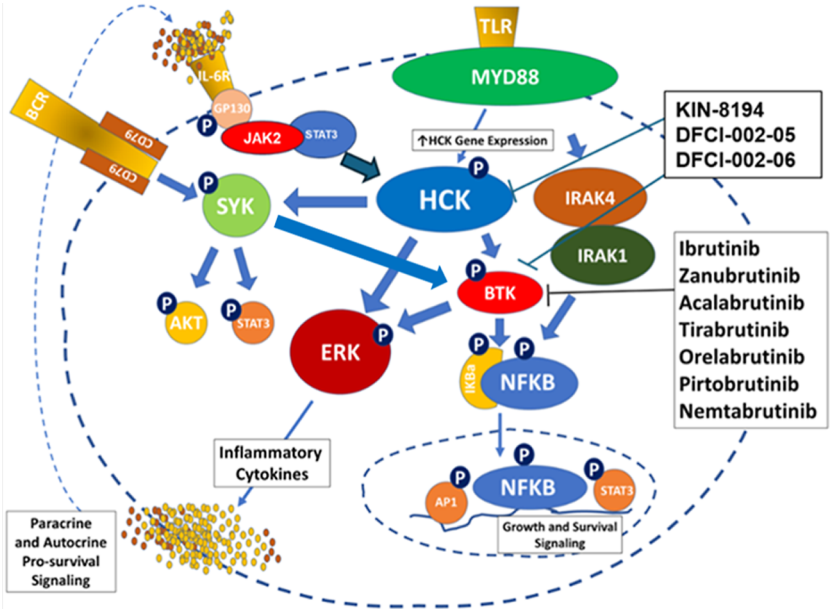

Figure 1. Mutated MYD88 Pro-Survival Signaling Pathways. Mutated MYD88 upregulates transcription and activates the SRC family member Hematopoietic Cell Kinase (HCK) which activates the BTK, SYK and ERK signaling cascades. Compounds that inhibit HCK, BTK or both are shown. DFCI-002-05 (**4**) and −06 (**5**) are bifunctional PROTACs that block kinase function and degrade both HCK and BTK. KIN-8194 is a kinase inhibitor and served as the scaffold for the development of DFCI-002-05 (**4**) and −06 (**5**).

inhibitor pirtobrutinib is clinically active in $MYD88^{Mut}$ WM patients and overcomes mutated BTK^{Cys481} acquired resistance to covalent BTK inhibitors.[16] Acquired mutations which abrogate pirtobrutinib binding can also lead to acquired resistance.[17]

Recent studies have identified BTK kinase impaired BTK-inhibitor resistance mutations that support downstream BCR signaling through noncatalytic scaffold functions by recruiting surrogate kinases such as HCK. Kinase-deficient BTK mutants, including $BTK^{Cys481Phe}$ and $BTK^{Cys481Trp}$ transactivate HCK via phosphotyrosine mediated interactions that disrupt HCK autoinhibition thereby enabling continued activation of PLCγ2 and NF-κB signaling.[18] This reciprocal signaling mechanism reinforces the importance of dual BTK and HCK targeting in $MYD88^{Mut}$ driven lymphomas. While current therapeutic strategies focus primarily on BTK inhibition, these approaches do not address upstream activation of BTK by HCK, nor do they extinguish parallel survival pathways involving ERK, SYK and AKT signaling. Together, these findings underscore the limitations of targeting BTK alone, particularly in the context of resistance mutations that engage upstream or compensatory pathways. Taken together, these findings support a therapeutic strategy based on targeted HCK protein degradation to comprehensively dismantle oncogenic signaling. Unlike kinase inhibitors, proteolysis targeting chimeras (PROTACs) eliminate the protein target entirely, disrupting both catalytic and noncatalytic functions. Prior work in receptor tyrosine kinases (RTKs) and B cell signaling proteins have demonstrated that targeted degradation can yield more durable suppression of oncogenic signaling by eliminating both catalytic and non-catalytic scaffold functions. This approach may overcome resistance not only from kinase domain mutations but also from kinome rewiring, a process in which cancer cells adaptively activate alternative kinases or signaling pathways to bypass the inhibited target and maintain survival.

Several BTK-targeting PROTACs have been developed to overcome resistance associated with BTK mutations. BGB-16673 is an orally administered cereblon-recruiting degrader that targets both wild-type BTK (BTK^{WT}) and mutated BTK associated with resistance to covalent and noncovalent BTK inhibitors. BGB-16673 has shown high levels of activity in relapsed and refractory WM.[19] NX-5948 is also an orally directed BTK-directed degrader which in early studies has shown high levels of activity in WM.[20] An acquired mutation in BTK ($BTK^{Ala428Asp}$) is associated with clinical resistance to BGB-16673, as well as other covalent and noncovalent BTK inhibitors.[21] These studies highlight the feasibility of BTK degradation as a therapeutic strategy. However, they were not designed to address upstream SRC-family kinases such as HCK, which contribute to BTK activation and additional pro-survival signaling pathways in $MYD88^{Mut}$ lymphomas (Figure 1). Accordingly, our aim was to determine whether dual degradation of HCK and BTK provides functional benefit relative to dual inhibition with the previously reported dual inhibitor KIN-8194.[22]

RESULTS

Using the KIN-8194 scaffold as a starting point, we developed PROTACs directed against HCK and BTK. KIN-8194 was selected as the starting scaffold because it is a potent, noncovalent dual inhibitor of BTK and HCK that retains activity against the clinically relevant BTK^{C481S} mutant.[22] The compound features a solvent-exposed piperazine moiety that is synthetically accessible. These attributes made KIN-8194 an ideal core for PROTAC development, allowing linker attachment through the distal piperazine nitrogen while maintaining balanced inhibition of both targets. To refine potency and selectivity, we carried out a focused structure−activity relationship (SAR) study that explored modifications to the core scaffold, linker chemistry and length, pomalidomide attachment site, and E3 ligase recruiter interactions. Representative analogues from these efforts are shown in Figures 2 and 3.

https://doi.org/10.1021/acs.jmedchem.5c02444
J. Med. Chem. 2026, 69, 1119−1134

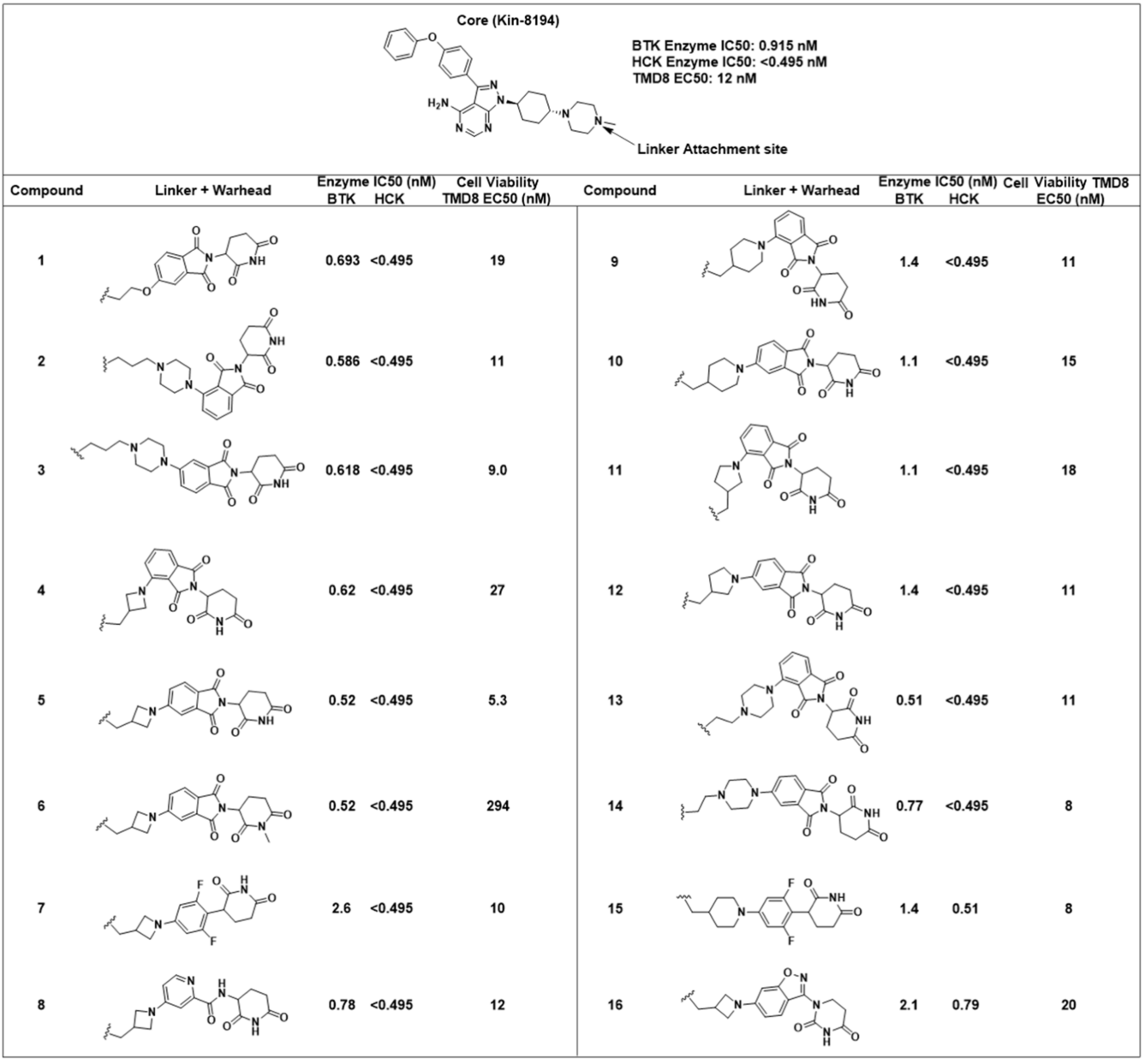

Compound	Linker + Warhead	Enzyme IC50 (nM) BTK	HCK	Cell Viability TMD8 EC50 (nM)
1		0.693	<0.495	19
2		0.586	<0.495	11
3		0.618	<0.495	9.0
4		0.62	<0.495	27
5		0.52	<0.495	5.3
6		0.52	<0.495	294
7		2.6	<0.495	10
8		0.78	<0.495	12
9		1.4	<0.495	11
10		1.1	<0.495	15
11		1.1	<0.495	18
12		1.4	<0.495	11
13		0.51	<0.495	11
14		0.77	<0.495	8
15		1.4	0.51	8
16		2.1	0.79	20

Figure 2. Development of HCK/BTK PROTACs utilizing the KIN-8194 scaffold. Analogues of PROTACs developed and whose structure activity relationships were investigated in these studies are shown. Enzymatic IC_{50} (nM) and cell viability EC_{50} (nM) in $MYD88^{Mut}$ TMD8 ABC DLBCL lymphoma cells are shown. KIN-8194 core is shown above PROTACs.

Guided by computational modeling performed in molecular operating environment (MOE) using the X-ray crystal structures of HCK (PDB ID: 5ZJ6)[22] and cereblon bound to pomalidomide (PDB ID: 6H0F)[23] we prioritized shorter linkers predicted to maintain an interligand distance of approximately 6−8 Å between the piperazine nitrogen of the KIN-8194 warhead and the aryl ring of pomalidomide with one pose shown in Figure 4.

Linkers within this distance range were predicted to favor productive ternary complex formation between BTK, HCK, and cereblon while minimizing linker strain and misalignment. Consistent with prior findings that the cyclohexyl ring within the KIN-8194 scaffold was critical for maintaining high enzymatic potency, this structural element was preserved throughout PROTAC development. Additionally, to explore the impact of cereblon engagement geometry on neo-substrate recruitment, we systematically varied linker attachment at either the 4- or 5-position of the pomalidomide aryl ring. Previous studies have shown that 4-position attachment favors degradation of IKZF1 and IKZF3, while 5-position linkers tend to minimize neo-substrate recruitment.[24] However, these conclusions were based primarily on linear alkyl and PEG linkers. In our study, we sought to determine whether these positional effects extend to PROTACs bearing short, rigid linkers connected via small heterocyclic rings, such as azetidine and piperazine, which impose distinct geometric constraints on cereblon engagement. This approach allowed us to confirm whether previously reported positional effects also applied in the context of dual BTK/HCK degraders. Compounds were evaluated for their effects on cell proliferation in both $MYD88^{Mut}$ TMD8 and BCWM.1 cells. However, prioritization decisions during SAR optimization were based primarily on TMD8 EC_{50} values. While

https://doi.org/10.1021/acs.jmedchem.5c02444
J. Med. Chem. 2026, 69, 1119−1134

Compound	Structure	Enzyme IC50 (nM) BTK	Enzyme IC50 (nM) HCK	Cell Viability TMD8 EC50 (nM)
17	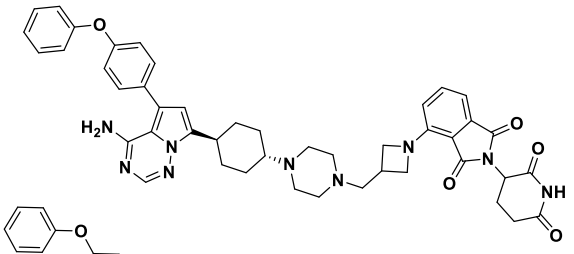	9.2	1.1	54
18	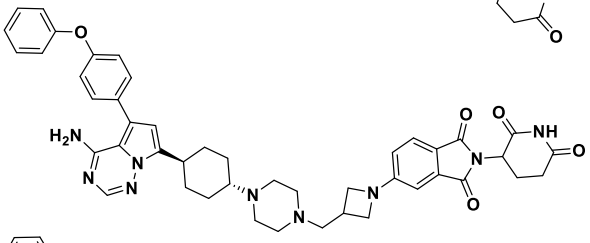	2.7	<0.495	27
19	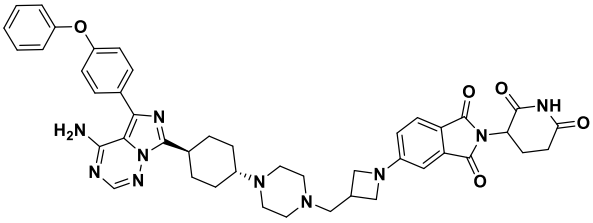	1.4	<0.495	100
20	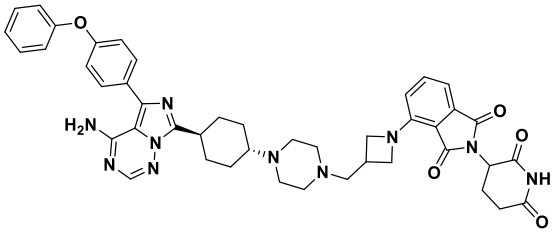	0.9	<0.495	10

Figure 3. Structure Activity Analysis for HCK/BTK PROTACs with Different Cores and E3 Ligase Warheads developed from KIN-8194 scaffold. Enzymatic IC_{50} (nM) and cell viability EC_{50} (nM) in $MYD88^{Mut}$ TMD8 ABC DLBCL lymphoma cells are shown.

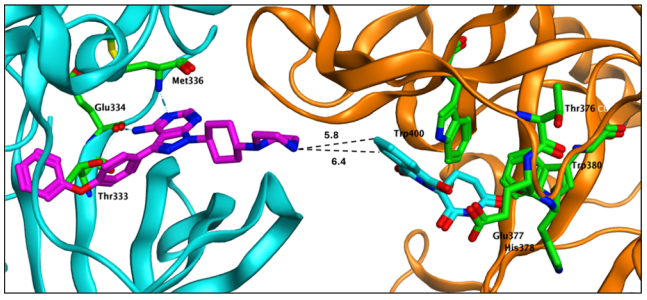

Figure 4. Computational modeling used to support PROTAC development from KIN-8194. Computational model of CRBN (orange)/HCK (cyan) with a truncated derivative of pomalidomide (blue) and a truncated derivative of KIN-8194 (pink). The distance between the two ligands in this pose (5.8–6.4 A) is highlighted.

strong inhibitory effects were observed in BCWM.1 cells, dose–response curves frequently deviated from classical sigmoidal behavior, resulting in unreliable EC_{50} curve fits. This variability likely reflects the distinct biological characteristics of BCWM.1 cells, including slower proliferation rates and increased reliance on microenvironmental signaling, which may attenuate the direct impact of BTK and HCK degradation. In contrast, TMD8 cells exhibited robust $MYD88^{Mut}$ driven BTK/HCK dependency and produced consistent, interpretable dose–response relationships. Accordingly, compounds demonstrating improved cellular potency relative to KIN-8194 in TMD8 cells were prioritized for further characterization of BTK and HCK degradation.

Initial SAR exploration revealed that short alkyl linkers consisting of two carbons attached to pomalidomide via an oxygen atom (e.g., **1**) maintained subnanomolar enzyme inhibition of both BTK and HCK; however, this compound exhibited reduced ability to inhibit cell proliferation in TMD8 cells compared to KIN-8194. We then investigated longer linkers, including **2** and **3**, both of which incorporated a C3 alkyl chain attached to pomalidomide through a piperazine ring. These compounds maintained subnanomolar enzyme potency but exhibited similar cellular antiproliferative potency as KIN-8194 in TMD8 cells. Nevertheless, to increase the likelihood of developing orally active PROTACs, we sought to rigidify the linker system further. This led to the synthesis of **13** and **14**, which both feature a C2 alkyl chain connected via a piperazine ring, as well as **4** and **5** (hereafter referred to as **DFCI-002-06**), which employ even shorter C1 azetidine linkers. Compounds **13** and **14** demonstrated similar or slightly reduced potency relative to KIN-8194 in TMD8 proliferation assays; however, **DFCI-002-06** showed increased potency relative to KIN-8194. This suggested a possible improvement in HCK/BTK degradation driven effects over HCK/BTK kinase inhibition alone. To further probe structure–activity relationships, we prepared an additional series of compounds (7-12, 15-20) incorporating

https://doi.org/10.1021/acs.jmedchem.5c02444
J. Med. Chem. 2026, 69, 1119–1134

diverse linkers, alternative attachment geometries, different E3 ligase recruiting warheads, and even core scaffolds distinct from KIN-8194. While these analogs expanded the chemical space examined, none provided a clear improvement cellular activity relative to **DFCI-002-06**. Consequently, they were not advanced to detailed mechanistic studies. These results confirmed **DFCI-002-06** as our lead degrader since it showed superior potency in TMD8 cells versus other analogs as well as KIN-8194. Although **4** did not outperform KIN-8194 in initial TMD8 antiproliferative assays, it was included in subsequent biological testing since it differed only in pomalidomide attachment at the 4-position of the aryl ring. This design allowed us to investigate whether altering cereblon engagement geometry could influence neo-substrate recruitment and degradation.

To assess whether the optimized geometry of **DFCI-002-06** would enable productive ternary complex formation, we performed molecular docking into a modeled HCK−cereblon complex, the key interface relevant to its proposed mechanism of action. The resulting ternary pose revealed that **DFCI-002-06** simultaneously engaged both HCK and cereblon with favorable spatial alignment and minimal linker strain (Figure 5). Notably,

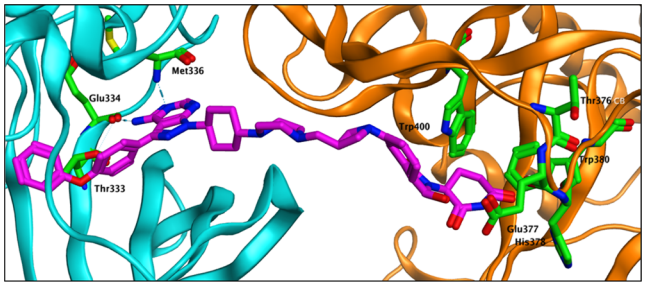

Figure 5. Computational model of ternary complex formation by 5 (DFCI-002-06) with HCK and cereblon. Modeled ternary complex of HCK (Cyan), Cereblon (Orange), and **5** (Purple) are shown. Binding site residues are depicted (Green).

the interligand distance observed in the docking model (6−7 Å) closely matched the optimal spacing predicted by our earlier computational modeling, further validating the design rationale for a short, rigid linker. These results support the feasibility of productive ternary complex formation and provide a structural basis for the enhanced activity of **DFCI-002-06** relative to analogs with alternate linker geometries.

To validate target engagement and assess the functional consequences of degradation, we evaluated the effects of **4** and **DFCI-002-06** on protein levels of HCK and BTK in BCWM.1 and TMD8 cells. Western blot analysis demonstrated that **DFCI-002-06** induced potent, concentration-dependent degradation of HCK and BTK at 0.1−0.5 μM in wild-type TMD8 and BCWM.1 cells (Figure 6A). The extent of degradation varied modestly between the two lines, with BTK degradation more pronounced in TMD8 and HCK degradation more complete in BCWM.1. These patterns may reflect differences in protein expression or degradation machinery across lines. In BCWM.1 cells, viability responses were nonsigmoidal, consistent with the slower growth kinetics and inherent heterogeneity of this patient-derived model, and therefore precluded reliable EC_{50} determination. Nonetheless, **DFCI-002-06** elicited strong apoptotic and antiproliferative effects relative to Kin-8194, confirming robust target engagement and functional activity in a WM-relevant context. Taken together, the activity of **DFCI-002-06** in both TMD8 and BCWM.1 models supports the relevance of dual BTK/HCK degradation not only in ABC-DLBCL but also in Waldenström's Macroglobulinemia, where HCK is an established driver of $MYD88^{Mut}$ signaling.**DFCI-002-06** In TMD8 and BCWM.1 cells engineered to express mutated BTK ($BTK^{Cys481Ser}$), **DFCI-002-06** also promoted efficient dual degradation of HCK and BTK at a concentration of 1 μM, thereby confirming activity against this frequently acquired resistance mutation to covalent BTK inhibitors (Figure 6B). We also evaluated **4** in wild-type BTK (BTK^{WT}) and HCK (HCK^{WT}) TMD8 and BCWM.1 cells, wherein it degraded both HCK and BTK. However, at higher concentrations **4** exhibited a pronounced "hook effect" against both targets characterized by partial recovery of these protein levels (Figure 6A). Conversely, **6**, a nondegrading compound with an *N*-methyl glutarimide to abolish cereblon binding, showed no measurable degradation on HCK or BTK at any tested concentration, confirming the cereblon dependency for **DFCI-002-06** mediated degradation (Figure 6A,B). Quantitative

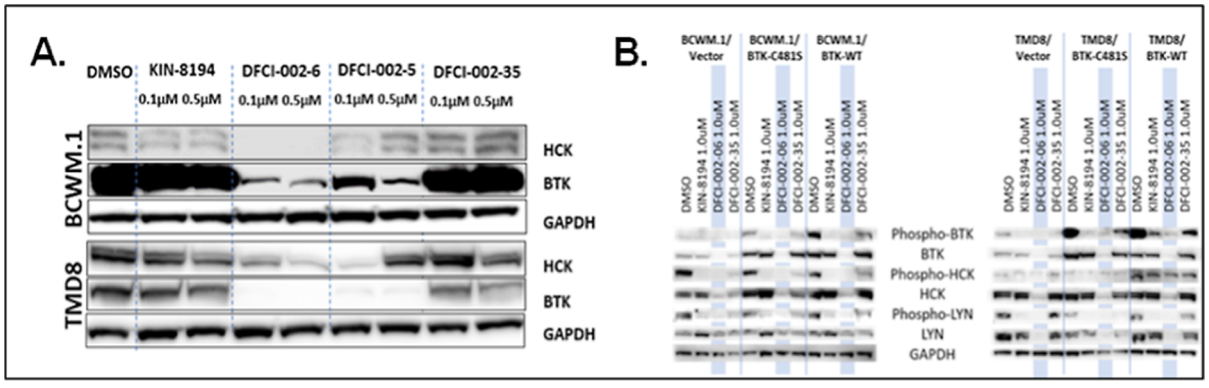

Figure 6. Western Blot Analysis for changes in protein levels and activation following treatment with KIN-8194, DFCI-002-06, Compound 4 (DFCI-002-05) and Compound 6 (DFCI-002-35). (A) Changes in total protein levels for indicated proteins in MYD88 mutated BCWM.1 and TMD8 following treatment with compounds at either 0.1 or 0.5 μM for 16 h. Compound 6 (DFCI-002-35), a nondegrading compound with an *N*-methyl glutarimide to abolish cereblon binding (**B**). Changes in phosphor- and total protein levels for indicated proteins in transduced BCWM.1 or TMD8 cells expressing vector alone, $BTK^{Cys481Ser}$ or BTK^{WT} following treatment with compounds at 1.0 μM for 16 h. Compound 6 (DFCI-002-35) contains an *N*-methyl-glutarimide modification that abolishes cereblon binding and serves as a nondegrading control. Representative results from a minimum of two independent experiments are shown.

https://doi.org/10.1021/acs.jmedchem.5c02444
J. Med. Chem. 2026, 69, 1119−1134

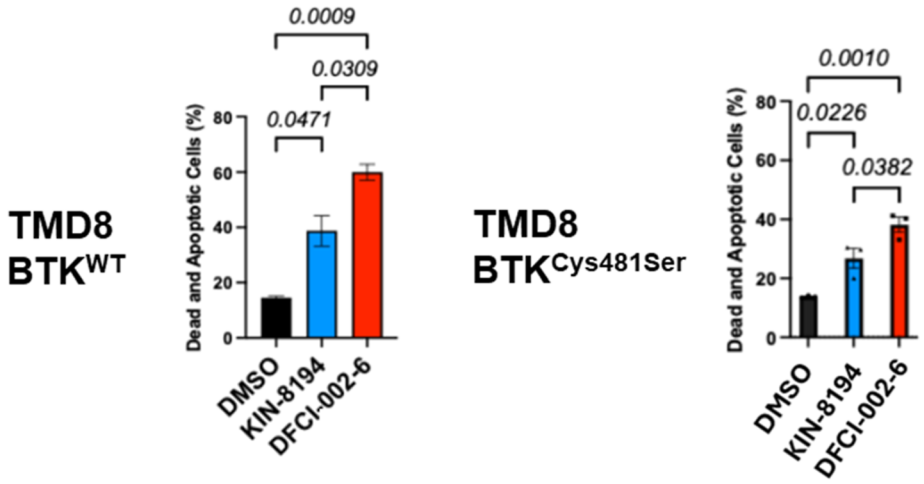

Figure 7. Apoptotic studies following treatment with KIN-8194 or DFCI-002-06. Apoptosis was assessed by Annexin V/Propidium Iodide (PI) staining transduced TMD cells expressing wild-type (n = 3) or mutated BTK ($BTK^{Cys481Ser}$) (n = 4) at 0.5 μM for 16 h. P-values for comparisons are shown in the Figure. DMSO, dimethyl sulfoxide.

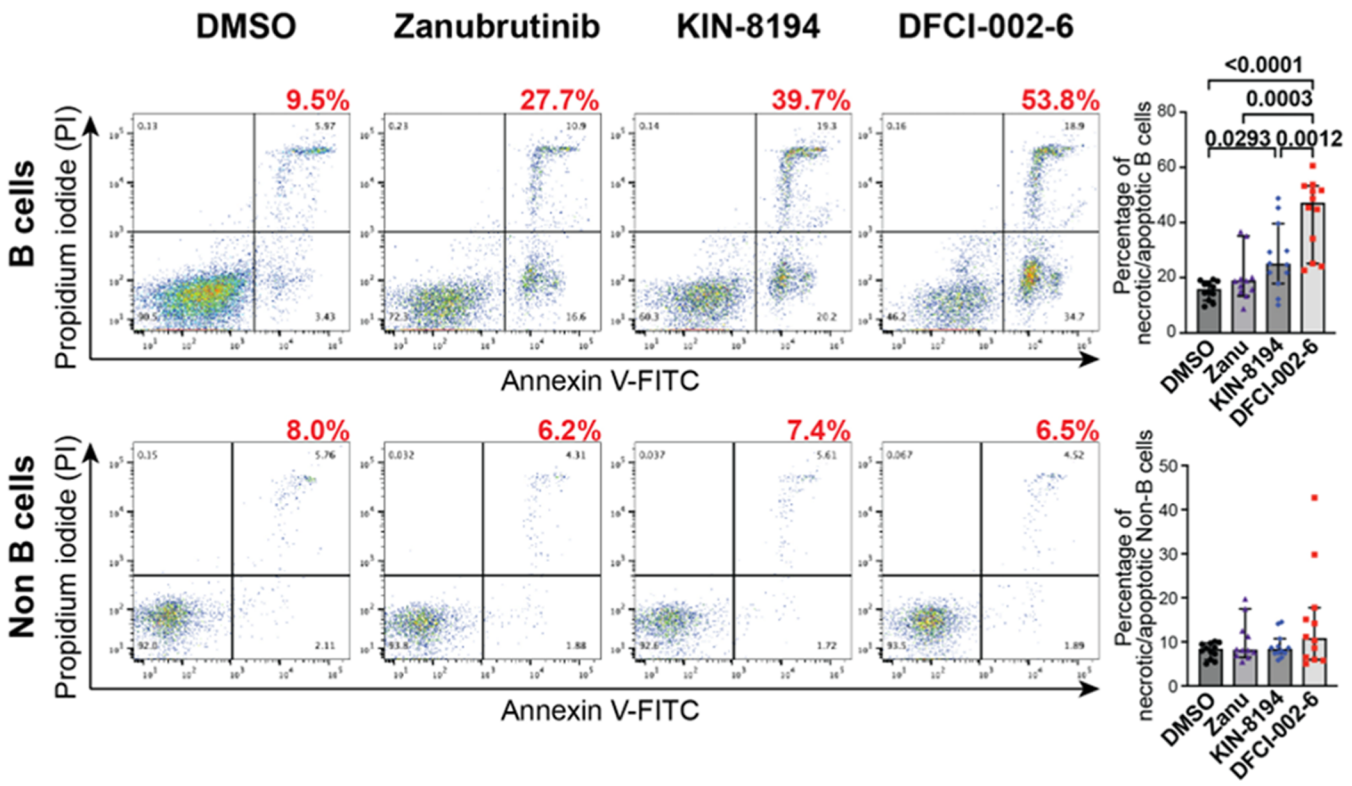

Figure 8. Apoptosis induction by **DFCI-002-06** in primary WM bone marrow cells. Bone marrow mononuclear cells from patients with Waldenström macroglobulinemia were treated with DMSO, zanubrutinib, KIN-8194, or **DFCI-002-06** (0.5 μM, 20 h). Apoptosis was assessed by flow cytometry using Annexin V-FITC/propidium iodide (PI) staining with gating on $CD19^+$ lymphoplasmacytic cells (LPCs) and $CD19^-$ non-B cells. DFCI-002-6 induced robust apoptosis in $CD19^+$ LPCs, significantly exceeding the effects of zanubrutinib and KIN-8194, while sparing $CD19^-$ non-B cells. Error bars represent median with 95% CI (n = 12 patients). Statistical analysis was performed using two-way ANOVA with Tukey's multiple comparisons test. Patient clinical characteristics are provided in Table 1.

degradation analyses were performed for **DFCI-002-06** and compound **4** to determine their half-maximal degradation concentrations (DC_{50}) and maximal degradation (D_{max}) values (Figure S6). Western blot densitometry across a 0.03−10 μM concentration range (16 h) yielded DC_{50} values of 4.5 nM for BTK and 1.3 nM for HCK, with D_{max} values of >95% for BTK and 87% for HCK for **DFCI-002-06**. Compound **4** showed slightly higher DC_{50} values of 7 nM for BTK and 5 nM for HCK compared to **DFCI-002-06** and also achieved >95% D_{max} for BTK; however, maximal degradation of HCK was substantially lower, with a D_{max} of only 53% and a pronounced hook effect at higher concentrations, consistent with reduced cereblon engagement efficiency inferred from its 4-position pomalidomide linkage. These findings confirm that **DFCI-002-06** achieves more efficient and sustained dual-target degradation within the pharmacologically relevant range observed in TMD8

https://doi.org/10.1021/acs.jmedchem.5c02444
J. Med. Chem. 2026, 69, 1119−1134

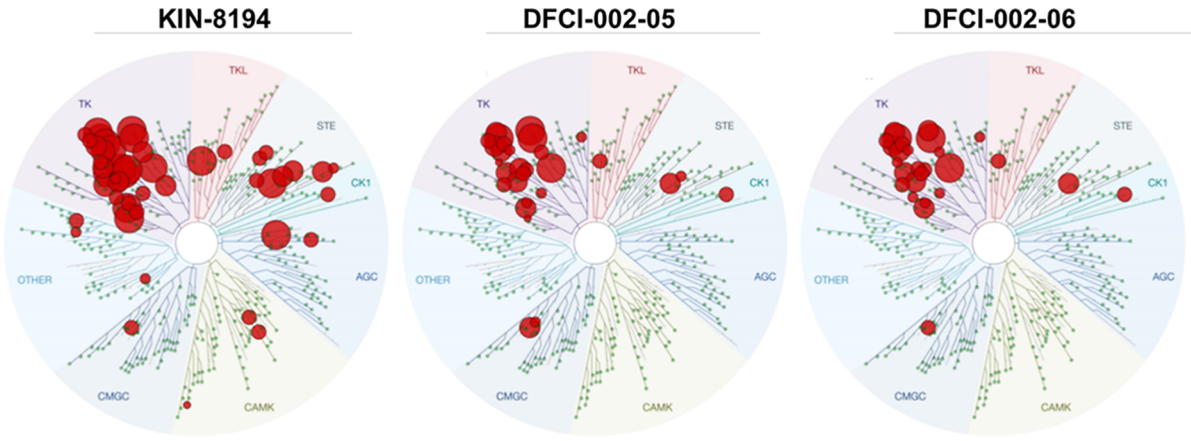

Figure 9. KINOMEscan results for KIN-8194, Compound 4 (DFCI-002-05) and DFCI-002-06. Kinome selectivity profile was generated against a diverse panel of 464 kinases using compounds at 1.0 μM. Kinases with inhibition of >90% are denoted in red circles. **Compound 4** and **DFCI-002-06** exhibited kinome selectivity S(10) scores of 8.7% and 8.5%, respectively, versus 15.8% for KIN-8194.

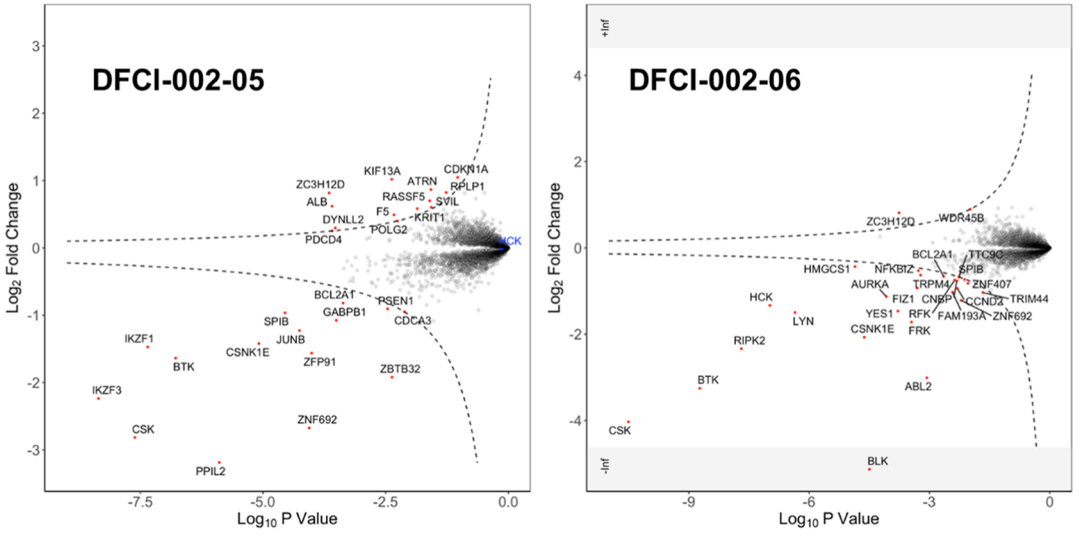

Figure 10. Global proteomics results for 4 (DFCI-002-05) and DFCI-002-06. Proteomics were performed in TMD8 cells following treatment with compounds at a concentration of 1.0 μM for 6 h. Log fold change in protein levels are shown.

viability assays. We next evaluated whether targeted degradation of HCK and BTK by **DFCI-002-06** induced apoptosis in BTK^{WT} and $BTK^{Cys481Ser}$ expressing TMD8 cells. Treatment of BTK^{WT} TMD8 cells at equimolar concentrations (0.5 μM) induced significantly higher levels of apoptosis following **DFCI-002-06** versus KIN-8194, the parental HCK/BTK inhibitor (Figure 7). Similarly, **DFCI-002-06** induced significantly higher levels of apoptosis than KIN-8194 in TMD8 cells expressing the $BTK^{Cys481Ser}$ mutation, with greater apoptotic activity observed at equimolar concentrations (0.5 μM; Figure 7). In addition to BTK and HCK, **DFCI-002-06** induced degradation of LYN in engineered BTK^{WT} and BTK^{C481S} TMD8 cells, where the effect was more pronounced and approached near-complete loss. By contrast, only partial LYN degradation was observed in BCWM.1 cells. While not a rational design target, this secondary effect may contribute to the therapeutic activity of **DFCI-002-06** in $MYD88^{Mut}$ lymphomas. These findings further support the advantage of dual HCK/BTK degradation over kinase inhibition alone.

To further evaluate the translational potential of **DFCI-002-06**, we tested its activity in primary bone marrow mononuclear cells isolated from patients with $MYD88^{L265P}$ mutations. Consistent with the cell line data, **DFCI-002-06** induced significantly higher levels of apoptosis in malignant $CD19^{+}$ lymphoplasmacytic cells compared to both Kin-8194 and zanubrutinib. Importantly, this activity was selective, as $CD19^{-}$ non-B cells were spared, underscoring a favorable therapeutic window. Notably, **DFCI-002-06** also demonstrated superior potency in patient samples harboring BTK resistance mutations, supporting its capacity to overcome both intrinsic and acquired resistance in a clinically relevant context (Figure 8).

We next assessed the kinome selectivity of **4** and **DFCI-002-06** utilizing the Eurofins KINOMEscan assay which assesses activity against a panel of 468 kinases. At a concentration of 1 μM, both **Compound 4** and **DFCI-002-06** exhibited greater kinome selectivity with S(10) scores of 8.7% and 8.5%, respectively, versus 15.8% for KIN-8194 (Figure 9). Complete KinomeSCAN results can be found in the Supporting Information section (Figure S5). The improvement is likely due to the increased steric bulk and altered physicochemical properties introduced by the PROTAC linker and E3 ligase warhead, including increased molecular weight, polar surface area, and reduced conformational flexibility. These features

https://doi.org/10.1021/acs.jmedchem.5c02444
J. Med. Chem. 2026, 69, 1119−1134

likely hinder nonspecific engagement with kinases that possess smaller ATP-binding pockets. Among the kinases that retained measurable binding affinity in the KINOMEscan panel was EGFR, a known off-target of ibrutinib and zanubrutinib associated with adverse effects such as rash and GI-upset.

To assess whether **4** and **DFCI-002-06** exhibited functional EGFR inhibition, we further evaluated these compounds in Ba/F3 cells engineered to express wild-type EGFR, a model system used to evaluate EGFR-dependent cytotoxicity. This model provides a clean system to assess EGFR-dependent cytotoxicity and does not represent a therapeutic disease model. Both degraders showed markedly reduced potency relative to ibrutinib and zanubrutinib in this assay, with IC_{50} values of 700 nM for **4** and 1380 nM for **DFCI-002-06**, compared to 15 nM and 52 nM for ibrutinib and zanubrutinib, respectively. These findings suggest that while EGFR may bind weakly to the degrader scaffold, this engagement does not result in significant functional inhibition. Thus, the EGFR off-target risk appears minimal for both PROTACs, further supporting the improved off-target profile of **DFCI-002-06** relative to clinically approved BTK inhibitors.

To evaluate the selectivity of degradation beyond BTK and HCK, we performed global proteomic profiling in TMD8 cells treated with **4** or **DFCI-002-06** for 6 and 16 h (Figure 10). Both compounds effectively degraded BTK, while only **DFCI-002-06** induced robust degradation of HCK, consistent with Western blot and cell viability data. In contrast, HCK was not significantly degraded by **4** in the proteomic data set, despite evidence of partial degradation by Western blot at lower concentrations. In Western blot analysis, HCK degradation by **4** was prominent at 0.1 μM and diminished at 0.5 μM. In contrast, the proteomics study was conducted at 1.0 μM, wherein no significant HCK degradation was observed, further suggesting a concentration-dependent hook effect. The Hook effect is likely due to its broader neo-substrate degradation profile—including IKZF1, IKZF3, and several zinc finger−containing transcription factors, which likely increase competition for cereblon and reduce degradation efficiency at higher concentrations. We recognize that global proteomics is not always a reliable indicator of degradation magnitude due to limitations in peptide coverage, digestion efficiency, and detection bias. These limitations are well documented in the context of targeted protein degradation, where MS-based proteomic workflows can be biased, low throughput, or incomplete, and therefore provide limited accuracy in assessing relative degradation efficiency. In contrast, Western blot analysis remains the most reliable method for quantifying degradation magnitude.[25,26] Degradation of neo-substrates indeed correlates with the orientation of the cereblon-binding moiety: **4** is tethered at the 4-position of the pomalidomide aryl ring, a configuration previously shown to favor ternary complex formation with IKZF family substrates. In contrast, **DFCI-002-06** is linked via the 5-position, which appears to restrict cereblon engagement and exclude IKZF1/3 degradation. These findings are consistent with previous studies with linear alkyl and PEG linkers[25] and extend their observations to PROTACs incorporating short, rigid linkers connected via azetidine and piperazine rings. In addition to its selective neo-substrate profile, **DFCI-002-06** demonstrated a remarkably clean degradation signature, with only three additional proteins significantly reduced: RIPK2, LYN, and CSK. Among these, LYN—a SRC-family kinase implicated in $MYD88^{Mut}$ signaling and resistance to BTK inhibitors—was further validated by Western blot (Figure 6B) and may contribute to the therapeutic efficacy of **DFCI-002-06**. LYN degradation was more pronounced in TMD8 cells, where it approached near-complete loss at higher concentrations, but was only partial in BCWM.1 cells. This effect, while reproducible, is secondary to the core design targets BTK and HCK and is not central to the mechanism of action of **DFCI-002-06**. Notably, LYN was not degraded by **4**, further distinguishing **DFCI-002-06** as the more effective degrader in MYD88-mutated B cell malignancies. While these exploratory findings suggest additional contributions to activity, BTK and HCK were the only targets intentionally prioritized throughout our design, validated in multiple orthogonal assays, and directly linked to functional outcomes in cell viability and apoptosis assays. To confirm that degradation of BTK and HCK by **DFCI-002-06** was cereblon- and proteasome-dependent, we performed rescue experiments using pharmacologic inhibitors of the ubiquitin−proteasome pathway. TMD8 cells were pretreated with MLN4924 (a NEDD8-activating enzyme inhibitor that blocks cullin-RING ligase activity) or ZXH-04-130[27] (a cereblon degrader) followed by treatment with **DFCI-002-06**. Bortezomib was initially evaluated as a proteasome control; however, it produced marked cytotoxicity in TMD8 cells even at low concentrations, precluding reliable interpretation of target recovery, and was therefore excluded from the final rescue panel. Pretreatment with MLN4924 or ZXH-04-130 rescued **DFCI-002-06**–induced degradation of both BTK and HCK, as assessed by Western blotting (Figure 11). Importantly, ZXH-04-130 does not fully deplete cereblon; therefore, only partial rescue was observed under this condition, consistent with residual E3-ligase activity. These findings confirm that degradation by **DFCI-002-06** occurs via cereblon-mediated recruitment to the E3 ligase complex and requires intact neddylation and proteasomal machinery. To evaluate the suitability of **DFCI-002-06** for in vivo and clinical development, we conducted cross-species pharmacokinetic (PK) studies in mouse, rat, dog, and hamster following both intravenous (IV) and oral (PO) administration. **DFCI-002-06** exhibited favorable PK properties across all species, with particularly strong oral exposure in mice.

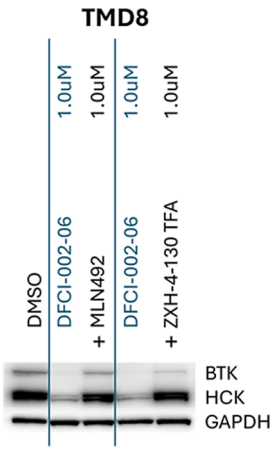

Figure 11. Degradation experiments for DFCI-002-06. Degradation rescue experiments were performed in TMD8 pretreated with either MLN4924 (a NEDD8-activating enzyme inhibitor that blocks cullin-RING ligase activity); or ZXH-04-130 (a cereblon degrader) followed by treatment with **DFCI-002-06**.

Following a single 10 mg/kg oral dose in mice, **DFCI-002-06** achieved a Cmax of 1.55 μM and an oral bioavailability of 39%,

https://doi.org/10.1021/acs.jmedchem.5c02444
J. Med. Chem. 2026, 69, 1119−1134

Table 1. Cross Species Pharmacokinetic Data for DFCI-002-06[a]

DFCI-02-6	mouse	rat	dog	hamster
CI_{obs}(mL/min/kg) following IV dose 2mpk (M) 5mpk (R,D,H)	2.43	14.5	8.24	12
AUC (min*mg/mL) 10 mpk PO	1.30×10^6	1.25×10^5	9.80×10^4	3.74×10^5
C_{max} (μM) 10 mpk PO	1.55	0.21	0.12	0.16
Vss_obs (L/kg)	1.97	6.5	11.2	10.1
F (%)	39	7.4	10	21

[a]Pharmacokinetic data are shown for mouse, rat, dog and hamster at the specified dose and route of administration.

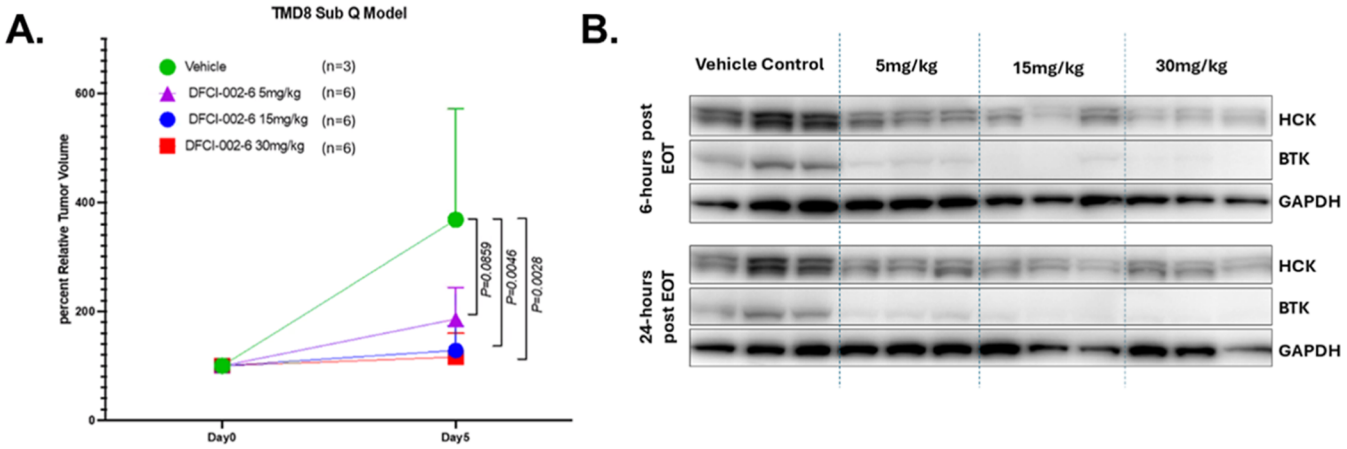

Figure 12. Pharmacodynamic study of orally administered DFCI-002-06 in TMD8 xenografted mice. Growth of xenografted TMD8 tumors was evaluated 5 days after oral administration of vehicle control ($n = 3$), or **DFCI-002-06** at 5, 15, 30 mg/kg ($n = 6$/each cohort) (**A**). Western blot analysis for BTK and HCK in lysates from TMD8 tumors harvested at 6 and 24 h following day 5 (final) dosing of vehicle control or **DFCI-002-06** at the indicated doses (**B**).

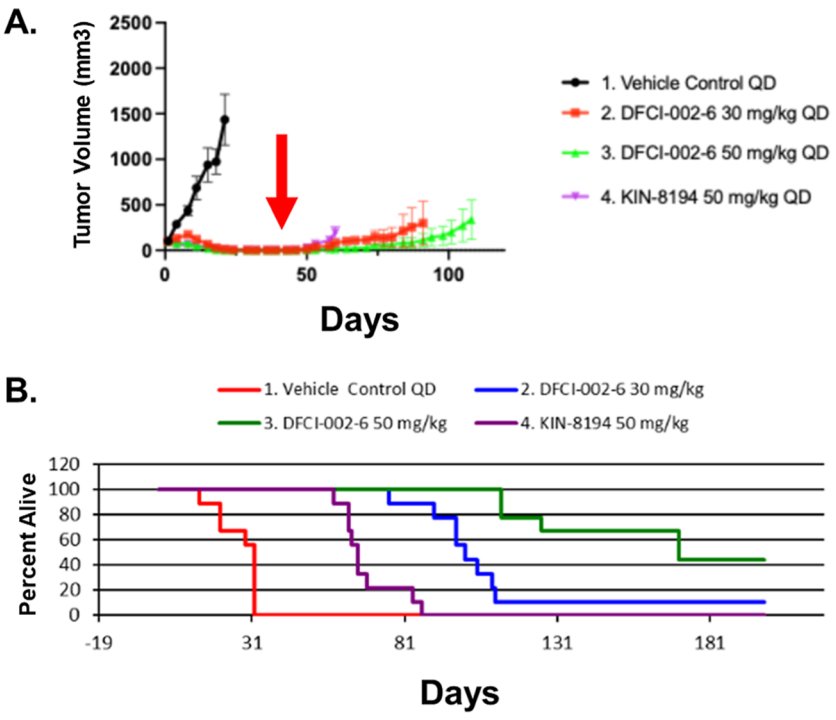

Figure 13. Efficacy assessments for DFCI-002-06 in TMD8 xenografted murine model. Tumor growth measurements are shown for xenografted mice (n = 9/cohort) treated daily with vehicle control, DFCI-002-06 (30 or 50 mg/kg), and KIN-8194 (50 mg/kg) administered orally for 6 weeks. Treatment was stopped at 6 weeks (red arrow) and xenografted mice assessed for tumor volume changes (**A**) and survival (**B**) for 12 additional weeks.

consistent with the relatively high oral absorption reported for other cereblon-based PROTACs in mice.[28] While these total plasma concentrations exceeded the in vitro degradation threshold (~0.5 μM; Figure 6A), **DFCI-002-6** exhibited very high plasma protein binding (>99%), limiting the free drug fraction (Tables S2−S6 where full in vitro ADME properties are summarized). In rats, dogs, and hamsters, oral exposure was more moderate, reflecting expected interspecies differences in

https://doi.org/10.1021/acs.jmedchem.5c02444
J. Med. Chem. 2026, 69, 1119−1134

clearance and half-life. Dose-escalation studies further revealed supraproportional increases in exposure between 30 and 60 mg/kg in mice, indicating nonlinear pharmacokinetics at higher doses (Figure S1, Table 1).

Based on the favorable pharmacokinetics and strong in vitro activity of **DFCI-002-06**, we next performed pharmacodynamic studies to evaluate on−target activity in tumor tissue and to inform dose selection for subsequent efficacy experiments. For this study, we assessed degradation of BTK and HCK within TMD8 xenograft tumors following oral administration of **DFCI-002-06** at either 5, 15, and 30 mg/kg for 5 days. We observed significant inhibition of tumor growth in xenografted mice that received 15 and 30 mg/kg of **DFCI-002-06**; $p = 0.0046$ and 0.0028 versus vehicle control treated mice, respectively (Figure 12A). Western blot analysis of tumors harvested at 6 and 24 h after the final dose on day 5 demonstrated robust dose dependent degradation of BTK and HCK, which was observed even outward to 24 h following the last dose consistent with drug levels observed in mice PK studies (Figure 12B). These results confirm that **DFCI-002-06** achieves potent and sustained degradation of BTK and HCK in vivo at pharmacologically achievable oral dosing, thereby demonstrating its therapeutic potential as an orally administrated agent.

Given the above pharmacodynamic study findings, we next evaluated the long-term therapeutic potential for **DFCI-002-06** in the TMD8 xenograft model. TMD8 xenografted mice received treatment with either vehicle control; KIN-8194 at 50 mg/kg; **DFCI-002-06** at 30 or 50 mg/kg by oral administration once daily for 6 weeks followed by a 12 week drug-free observation period to assess the durability of response. Although dual degradation of BTK and HCK was confirmed at lower doses (15 and 30 mg/kg) in short-term PD studies, the 50 mg/kg dose was selected for efficacy evaluation to ensure adequate tumor exposure and sustained pharmacodynamic effect. Treatment with **DFCI-002-06** at 30 and 50 mg/kg/daily, as well as KIN-8194 at 50 mg/kg/daily was well tolerated with no adverse events observed in NOD-SCID mice after 6 weeks of treatment.

Treatment with **DFCI-002-06** at either 30 or 50 mg/kg and KIN-8194 at 50 mg/kg showed near complete tumor suppression during active therapy while mice on vehicle control showed rapid tumor growth (Figure 13A). Importantly, **DFCI-002-06** demonstrated sustained tumor growth suppression, which was more pronounced in xenografted mice that received 50 versus 30 mg/kg. In contrast, mice treated with KIN-8194 showed tumor growth shortly after drug cessation. Overall survival paralleled tumor growth findings as shown in Figure 13B, with animals receiving **DFCI-002-06** showed a survival advantage over KIN-8194 or vehicle control, particularly for mice treated at 50 mg/kg/day.

To support the continued advancement of **DFCI-002-06** toward IND-enabling studies, we conducted a series of preclinical safety assessments, including genotoxicity, cardiac liability, and a 21 day rat toxicology study. In a mini-Ames assay using *Salmonella typhimurium* strains TA98 and TA100, **DFCI-002-06** was found to be nonmutagenic under all tested conditions. In glass-based whole-cell patch clamp assays, **DFCI-002-06** showed concentration-dependent inhibition of hERG current, with modest effects at 1−3 μM (25.8−39.0% inhibition) and stronger inhibition at $\geq$ 10 μM (62−77%) resulting in an IC_{50} of 5.2 μM. However, precipitation was observed at 10 and 30 μM, which might slightly underestimate the true IC_{50}. To further assess tolerability, a 21 day repeat-dose toxicity study was performed in Sprague−Dawley rats treated orally with **DFCI-002−06** at 50 mg/kg/day. The compound was well tolerated, with animals maintaining steady weight gain and no clinical signs of distress. Blood chemistry analyses revealed no treatment-related alterations in hepatic (ALT, AST, ALP, bilirubin) or renal (BUN, creatinine) function markers, and electrolyte and glucose levels remained within acceptable ranges. Hematology values were likewise unremarkable, with no evidence of cytopenias and only modest changes in leukocyte counts. A modest increase in spleen weight was noted, while all other organs were within normal ranges. Together, these findings support the favorable safety and tolerability profile of **DFCI-002-06** and justify its continued progression toward IND-enabling development. Raw data is available in the Supporting Information section.

DISCUSSION AND CONCLUSIONS

Herein, we describe the development of a first-in-class bifunctional PROTAC **DFCI-002-06** developed from KIN-8194, a dual BTK and HCK kinase inhibitor that we developed and characterized following a focused medicinal chemistry campaign.[23] **DFCI-002-06** showed potent degradation of BTK and HCK in vitro including in lymphoma cells engineered to express mutated BTK^{Cys481}, a mutation commonly associated with acquired covalent BTK-inhibitor resistance. While HCK degradation occurred to a lesser extent than BTK, both kinases were reproducibly degraded by **DFCI-002-06**, confirming that HCK degradation, though less potent, is a consistent feature of this scaffold. Importantly, **DFCI-002-06** also maintained potent kinase inhibitory activity against HCK and BTK akin to its parenteral scaffold, KIN-8194, in both wild-type and mutated BTK^{Cys481} expressing lymphoma cells. Our studies also demonstrated enhanced kinase selectivity of **DFCI-002-06** versus KIN-8194. Importantly, global proteomics screen showed limited off target effects for **DFCI-002-06**. Although multikinase degradation is a known feature of some PROTACs, **DFCI-002-06** represents, to our knowledge, the first degrader rationally developed to target both BTK and its upstream activator HCK, a design grounded in mechanistic studies of MYD88-mutated B cell signaling. We acknowledge that BTK dependence predominates in TMD8 cells. Nevertheless, **DFCI-002-06** showed an apoptotic advantage versus Kin-8194 and robust HCK degradation, supporting the premise that concurrent degradation of the upstream SRC-family kinase HCK can augment pathway suppression beyond BTK inhibition alone. This interpretation aligns with our prior pathway data positioning HCK upstream of BTK as well as in parallel pro-survival branches. Importantly, this study was not designed to benchmark **DFCI-002-06** against existing BTK degraders, which do not target HCK or LYN and were developed without consideration of upstream SRC-family inputs. Rather, our goal was to test whether dual degradation of BTK and HCK could provide additional benefit over dual kinase inhibition with KIN-8194. This dual-target rationale distinguishes **DFCI-002-06** from prior BTK degraders, which lack activity against non-catalytic SRC-family signaling nodes.

A key finding was the favorable bioavailability and pharmacokinetics observed with **DFCI-002-06** in cross species studies. A key pharmacokinetic finding was that **DFCI-002-6** is >99% bound to plasma proteins (Table S6), meaning free plasma concentrations are expected to be much lower than total levels measured in vivo. In addition, supraproportional pharmacokinetics were observed between 30 and 60 mg/kg in

https://doi.org/10.1021/acs.jmedchem.5c02444
J. Med. Chem. 2026, 69, 1119−1134

mice, suggesting nonlinear exposure at higher doses. This is relevant for the efficacy studies, which used 30 and 50 mg/kg dosing: although PK was not directly measured at 50 mg/kg, the nonlinear behavior at 60 mg/kg suggests that exposure increases between 30 and 50 mg/kg may also exceed dose-proportionality. Furthermore, pharmacodynamic studies were performed at 5−30 mg/kg, while efficacy studies used 30 and 50 mg/kg. Although matched PK/PD comparisons were not performed, degradation observed at 15−30 mg/kg supports the conclusion that pharmacologically relevant target engagement is achieved across the dosing range. The 50 mg/kg dose was therefore selected to ensure sustained tumor exposure and durability of effect, with nonlinear PK likely contributing to the enhanced suppression observed at this higher dose. Central to the in vivo assessments for **DFCI-002-06** were the pharmacodynamic studies showing robust degradation of HCK and BTK in xenografted $MYD88^{Mut}$ TMD8 lymphomas following oral administration of **DFCI-002-06**, activity which was well within pharmacologically achievable dosing. Efficacy studies in TMD8 xenografted mice were consistent with the pharmacodynamic studies. The goal of these studies was to test whether simultaneous degradation of BTK and HCK provides greater benefit than dual inhibition with KIN-8194, rather than to isolate the individual contribution of HCK degradation Both KIN-8194 and **DFCI-002-06** showed impressive antitumor activity in the TMD8 xenograft models, suppressing tumor growth during the active 6 week period of treatment. Indeed, even at 30 mg/kg, **DFCI-002-06** achieved tumor control during this period while tumors rapidly grew in xenografted mice treated with vehicle control. However, in the 12 week off treatment period that followed, xenografted mice treated with **DFCI-002-06**, particularly at the higher dosing of 50 mg/kg, showed superior outcomes in terms of tumor growth control as well as overall survival versus KIN-8194. While these findings suggest that continuous therapy with **DFCI-002-06** may be optimal over a time limited therapeutic approach, long-term disease was nonetheless recognized off treatment. The improved disease control off therapy may be related to longer intracellular residency, particularly since PROTACs can recycle and potentiate target depletion. In addition, degradation of target may destabilize pro-survival signaling associated with HCK and BTK, particularly in the setting of covalent BTK-inhibitor resistant disease. Dhami et al.[19] showed that certain mutated BTK^{Cys481} clones lose kinase activity, though downstream pro-survival signaling is maintained by BTK forming a scaffold with HCK via SH2 to propagate downstream pro-survival signaling. Similarly, we extended their findings to demonstrate scaffold dependence for HCK in other treatment related acquired BTK mutations with diminished BTK kinase activity such as $BTK^{Val416Leu}$, $BTK^{Ala428Asp}$, and $BTK^{Leu528Trp}$.[29]

In addition to HCK and BTK, the degradation of LYN by **DFCI-002-06** may also contribute to its activity. Hereto, the scaffold function of LYN may be critical to pro-survival signaling mediated by mutated MYD88. LYN expression is triggered by mutated MYD88 and increases in clones resistant to ibrutinib, while knockdown of LYN can abrogate resistance to ibrutinib.[30] These revelations particularly call out the potential use of **DFCI-002-06** in patients with $MYD88^{Mut}$ lymphomas who develop acquired resistance to BTK inhibitors. Finally, in preliminary safety testing, **DFCI-002-06** demonstrated no meaningful hERG inhibition and was nonmutagenic in Ames assays, and a 21 day repeat-dose rat toxicology study revealed no adverse findings across clinical chemistry or hematologic parameters. A modest, nonadverse increase in spleen weight observed in this study will be monitored in future GLP-compliant toxicology studies to determine whether this finding persists or progresses during longer-term dosing. Together, these findings provide further confidence in the translational potential of **DFCI-002-06** as a rational dual BTK/HCK degrader for $MYD88^{Mut}$ lymphomas.

EXPERIMENTAL SECTION

Synthetic Procedures

All reagents and solvents were purchased from commercial sources and used as received. Silica gel and reverse-phase flash column chromatography were conducted with Teledyne ISCO CombiFlash instruments and commercially available prepacked columns. Reverse-phase preparative high-pressure liquid chromatography (HPLC) purification of final analogues was performed over C18 columns with UV and MS detection using a MeCN/water gradient and TFA modifier. All compounds tested were of ≥95% purity by LCMS.

3-Iodo-1-(1,4-dioxaspiro[4.5]decan-8-yl)-1*H*-pyrazolo[3,4-*d*]pyrimidin-4-amine (22). To a suspension of 3-iodo-1*H*-pyrazolo[3,4-*d*]pyrimidin-4-amine (2.6 g, 10 mmol), 1,4-dioxaspiro[4.5]decan-8-ol (3.2 g, 20 mmol) and PPh_3 (3.9 g, 15 mmol) in THF (30 mL) was added dropwise DIAD (4.04 g, 20 mmol) over a period of 30 min at 0 °C. The reaction was stirred at room temperature for 12 h under nitrogen atmosphere. The reaction mixture was concentrated, and the residue was triturated with EtOAc (30 mL x 3), and the precipitate was dried in vacuo to give 3-iodo-1-(1,4-dioxaspiro[4.5]decan-8-yl)-1*H*-pyrazolo[3,4-*d*]pyrimidin-4-amine (2.8 g, 70%) as a white solid that was used without further purification. LCMS: m/z 402.0 $[M + H]^+$.

4-(4-Amino-3-iodo-1*H*-pyrazolo[3,4-*d*]pyrimidin-1-yl)-cyclohexan-1-one (23). To a suspension of 3-iodo-1-(1,4-dioxaspiro[4.5]decan-8-yl)-1*H*-pyrazolo[3,4-*d*]pyrimidin-4-amine (**22**) (2.8 g, 6.9 mmol) in THF (10 mL) was added HCl (6 N, 3 mL). The reaction was stirred at 60 °C for 2 h, and diluted with water. The aqueous phase was neutralized with saturated sodium carbonate solution to pH = 6−8, at which point a precipitate was formed. The precipitate was filtered and dried in vacuo to give 4-(4-amino-3-iodo-1*H*-pyrazolo[3,4-*d*]pyrimidin-1-yl)cyclohexan-1-one (2 g, 83% yield) as a white solid, which was used directly for the next step. LCMS: m/z 358.0 $[M + H]^+$.

***tert*-Butyl-4-((1*r*,4*r*)-4-(4-amino-3-iodo-1*H*-pyrazolo[3,4-*d*]-pyrimidin-1-yl)cyclohexyl)piperazine-1-carboxylate (24).** To a mixture of 4-(4-amino-3-iodo-1*H*-pyrazolo[3,4-*d*]pyrimidin-1-yl)-cyclohexan-1-one (23) (1.8 g, 5.05 mmol) in DCM (20 mL) was added *tert*-butyl piperazine-1-carboxylate (1.87 g, 10.11 mmol) and CH_3COOH (150 mg, 2.5 mmol). The resulting mixture was stirred at room temperature for 6 h, and then $NaHB(OAc)_3$ (2.14 g, 10.11 mmol) was added. The mixture was stirred at 50 °C overnight, and diluted with DCM (80 mL). The organic phase was washed with brine, dried over anhydrous Na_2SO_4, filtered and concentrated. The residue was purified by flash chromatography (silica, 40 g, 0−10% DCM\MeOH = 10:1 in DCM) to give *tert*-butyl-4-((1*r*,4*r*)-4-(4-amino-3-iodo-1*H*-pyrazolo-[3,4-*d*]pyrimidin-1-yl)cyclohexyl)piperazine-1-carboxylate (400 mg) as a white solid. LCMS: m/z 528.0 $[M + H]^+$.

***tert*-Butyl-4-((1*r*,4*r*)-4-(4-amino-3-(4-phenoxyphenyl)-1*H*-pyrazolo[3,4-*d*]pyrimidin-1-yl)cyclohexyl)piperazine-1-carboxylate (25).** To a mixture of *tert*-butyl-4-((1*r*,4*r*)-4-(4-amino-3-iodo-1*H*-pyrazolo[3,4-*d*]pyrimidin-1-yl)cyclohexyl)piperazine-1-carboxylate (24) (400 mg, 0.76 mmol) in dioxane/H_2O (20/2 mL) was added 4,4,5,5-tetramethyl-2-(4-phenoxyphenyl)-1,3,2-dioxaborolane (450 mg, 1.52 mmol), $Pd(dppf)Cl_2$ (55 mg, 0.076 mmol) and Na_2CO_3 (161 mg, 1.52 mmol). The resulting mixture was stirred at 90 °C for 12 h under nitrogen atmosphere and concentrated, and the residue was purified by flash chromatography (silica, 40 g, 0−10% MeOH in EtOAc) to give 4-((1*r*,4*r*)-4-(4-amino-3-(4-phenoxyphenyl)-1*H*-pyrazolo[3,4-*d*]pyrimidin-1-yl)cyclohexyl)piperazine-1-carboxylate (390 mg, 90% yield) as a white solid. LCMS: m/z 570.2 $[M + H]^+$.

https://doi.org/10.1021/acs.jmedchem.5c02444
J. Med. Chem. 2026, 69, 1119−1134

Scheme 1. Chemical Synthesis Steps for DFCI-002-06[a–h]

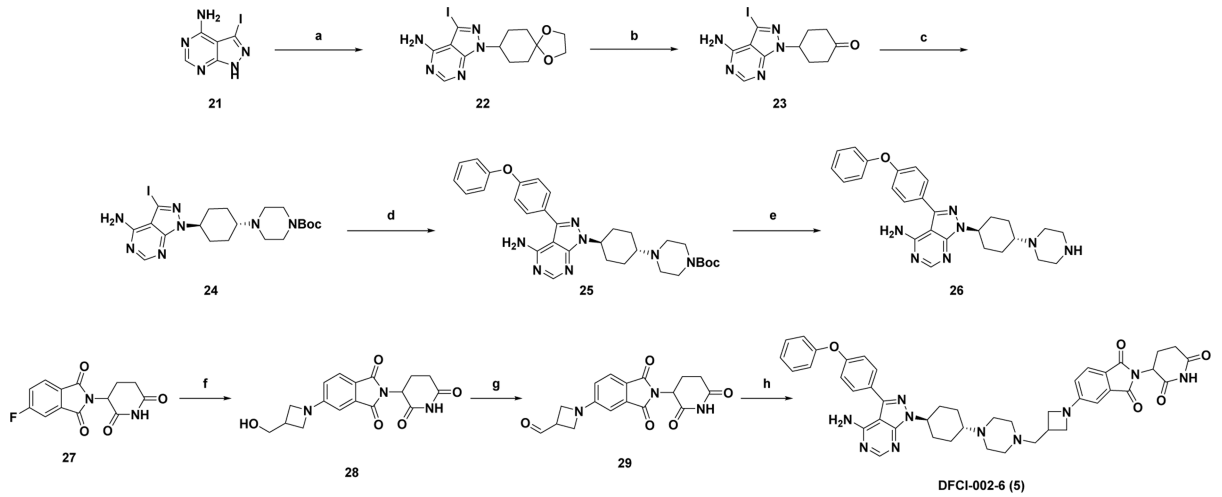

[a]1,4-dioxaspiro[4.5]decan-8-ol, Diisopropyl azodicarboxylate (DIAD), Triphenylphosphine (PPh_3), Tetrahydrofuran (THF). [b]6 N HCl, THF. [c]*tert*-butyl piperazine-1-carboxylate, sodium triacetoxyborohydride ($NaHB(OAc)_3$), dichloromethane (DCM), acetic acid. [d]4,4,5,5-tetramethyl-2-(4-phenoxyphenyl)-1,3,2-dioxaborolane, dichlorobis[(1,1′-bis(diphenylphosphino)ferrocene)]palladium(II) ($Pd(dppf)Cl_2$), sodium carbonate (Na_2CO_3), 1,4-dioxane/water. [e]HCl/dioxane/DCM. [f]N,N-Dimethylformamide (DMF), azetidin-3-ylmethanol, n,n-diisopropylethylamine (DIEA) 100 °C. [g]Dess–Martin periodinane (DMP), DCM. [h]**26**, $NaHB(OAc)_3$, DCM, acetic acid.

3-(4-phenoxyphenyl)-1-((1*r*,4*r*)-4-(piperazin-1-yl)-cyclohexyl)-1*H*-pyrazolo[3,4-*d*]pyrimidin-4-amine (26). To a mixture of 4-((1*r*,4*r*)-4-(4-amino-3-(4-phenoxyphenyl)-1*H*-pyrazolo-[3,4-*d*]pyrimidin-1-yl)cyclohexyl)piperazine-1-carboxylate (**25**) (390 mg, 0.68 mmol) in DCM (10 mL) was added HCl/dioxane (5 mL). The resulting mixture was stirred at room temperature overnight and diluted with DCM (40 mL). The organic phase was washed with saturated sodium hydrogen carbonate solution, brine, dried over anhydrous Na_2SO_4, filtered and concentrated to give 3-(4-phenoxyphenyl)-1-((1*r*,4*r*)-4-(piperazin-1-yl)cyclohexyl)-1*H*-pyrazolo[3,4-*d*]pyrimidin-4-amine (270 mg, 85% yield) as a white solid, which was used directly for the next step. LCMS: *m*/*z* 470.2 $[M + H]^+$.

2-(2,6-Dioxopiperidin-3-yl)-5-(3-(hydroxymethyl)azetidin-1-yl)isoindoline-1,3-dione (28). A mixture of 2-(2,6-dioxopiperidin-3-yl)-5-fluoroisoindoline-1,3-dione (400 mg, 1.45 mmol), azetidin-3-ylmethanol (189 mg, 2.17 mmol) and DIEA (461 mg, 4.35 mmol) in DMF (4 mL) was stirred at 100 °C for 16 h. After cooling to room temperature, the mixture was diluted with H_2O (20 mL), and the aqueous phase was extracted with EtOAc (20 mL X 3). The combined organic phase was washed with brine (30 mL), dried over anhydrous Na_2SO_4 and concentrated. The residue was purified by silica gel column (0–15% $MeOH/CH_2Cl_2$) to give 240 mg of 2-(2,6-dioxopiperidin-3-yl)-5-(3-(hydroxymethyl)azetidin-1-yl)isoindoline-1,3-dione as yellow solid (48% yield). LCMS: *m*/*z* 344.1 $[M + H]^+$.

1-(2-(2,6-dioxopiperidin-3-yl)-1,3-dioxoisoindolin-5-yl)-azetidine-3-carbaldehyde (29). A mixture of 2-(2,6-dioxopiperidin-3-yl)-5-(3-(hydroxymethyl)azetidin-1-yl)isoindoline-1,3-dione (240 mg, 0.70 mmol), Dess-Martin reagent (593 mg, 1.40 mmol) in DCM (5 mL) was stirred at 0 °C for 2 h. The mixture was quenched with a solution of $NaHCO_3$ and $Na_2S_2O_3$. The aqueous phase was extracted with DCM, and the organic phase was washed with brine, dried over anhydrous Na_2SO_4, and concentrated to give 600 mg of 1-(2-(2,6-dioxopiperidin-3-yl)-1,3-dioxoisoindolin-5-yl)azetidine-3-carbaldehyde as yellow solid (100% yield), which was used directly for the next step. LCMS: *m*/*z* 342.1 $[M + H]^+$.

5-(3-((4-((1*r*,4*r*)-4-(4-amino-3-(4-phenoxyphenyl)-1*H*-pyrazolo[3,4-*d*]pyrimidin-1-yl)cyclohexyl)piperazin-1-yl)-methyl)azetidin-1-yl)-2-(2,6-dioxopiperidin-3-yl)isoindoline-1,3-dione (DFCI-002-06). A mixture of 1-(2-(2,6-dioxopiperidin-3-yl)-1,3-dioxoisoindolin-5-yl)azetidine-3-carbaldehyde (29) (77 mg, 0.22 mmol), 3-(4-phenoxyphenyl)-1-((1*r*,4*r*)-4-(piperazin-1-yl)-cyclohexyl)-1*H*-pyrazolo[3,4-*d*]pyrimidin-4-amine (26) (70 mg, 0.15 mmol) and CH_3COOH (5 drops) was added to DCM (3 mL). The mixture was stirred at room temperature for 0.5 h, and then $NaBH(OAc)_3$ (95 mg, 0.45 mmol) was added, and the mixture was stirred at the room temperature overnight. The reaction mixture was diluted with H_2O (20 mL), and the aqueous phase was extracted with DCM (20 mL × 3). The organic phases was washed with brine (20 mL), dried over anhydrous Na_2SO_4, concentrated, and the residue was purified by silica gel chromatography (0–20% $MeOH/CH_2Cl_2$) to give 23 mg of 5-(3-((4-((1*r*,4*r*)-4-(4-amino-3-(4-phenoxyphenyl)-1*H*-pyrazolo[3,4-*d*]pyrimidin-1-yl)cyclohexyl)piperazin-1-yl)methyl)-azetidin-1-yl)-2-(2,6-dioxopiperidin-3-yl)isoindoline-1,3-dione as yellow solid (19% yield). LCMS: *m*/*z* 795.1 $[M + H]^+$. ^1H NMR (400 MHz, MeOD-d_4) δ 8.24 (s, 1H), 7.65 (dd, *J* = 13.7, 8.5 Hz, 3H), 7.46–7.35 (m, 2H), 7.26–7.05 (m, 5H), 6.80 (d, *J* = 2.1 Hz, 1H), 6.64 (d, *J* = 8.4 Hz, 1H), 5.13–4.99 (m, 2H), 4.30–4.09 (m, 2H), 3.85–3.65 (m, 2H), 3.21–2.56 (m, 14H), 2.30–2.06 (m, 8H), 1.76–1.51 (m, 2H). (Scheme 1)

Cell Models

$MYD88^{Mut}$ WM (BCWM.1) and ABC DLBCL (TMD8) cell lines were used in drug evaluations. $BTK^{Cys481Ser}$ expressing TMD8 cell lines were also evaluated, whose development and characterization we previously described.[23] Primary $CD19^+$ LPL cells were isolated from the bone marrow (BM) of WM patients as before.[23] Sample collection and use was approved by the Dana Farber/Harvard Cancer Center IRB, following patient consent.

Kinase Profiling

KINOMEscan assays were conducted at Eurofins DiscoverX Corporation (San Diego, CA).

Enzyme Assay

Enzymatic assays for BTK and HCK were performed by Invitrogen (Thermo Fisher Scientific) using validated in vitro kinase-activity protocols in accordance with the manufacturer's standard assay format.

Proteomics Assay

Cells were lysed in 8 M urea/50 mM HEPES, pH 8 via bead beating and lysates were clarified by centrifugation. An aliquot containing 50 μg protein was removed and subjected to reduction and alkylation in 5 mM dithiothreitol and 10 mM iodoacetamide. Proteins were precipitated with methanol and chloroform. Pellets were resuspended in 8 M urea and diluted 5x with 200 mM EPPS prior to digestion with trypsin at a 1:50 ratio of enzyme to protein at 32 °C overnight. Digests were acidified with formic acid (pH 3), desalted over SOLAμ elution plates

https://doi.org/10.1021/acs.jmedchem.5c02444
J. Med. Chem. 2026, 69, 1119–1134

(Thermo Fisher Scientific, Massachusetts, United States), and dried in a vacuum concentrator.

Data were collected using a TimsTOF Ultra (Bruker Daltonics, Bremen, Germany) coupled to a nanoElute2 LC pump (Bruker Daltonics, Bremen, Germany) via a CaptiveSpray nanoelectrospray source. Peptides were separated on a reversed-phase C18 column (25 cm × 75 μM ID, 1.6 μ , IonOpticks, Australia) with an integrated captive spray emitter. Peptides were separated using a 50 m n gradient of 2−30% buffer B (99.9% acetonitrile, 0.1% formic acid) with a flow rate of 250 n /min and column temperature maintained at 50 °C. Mass spectra were collected in diaPASEF mode, with 25 Da two windows in each 50 m scan, defined between 400−1200 m z and 1/k0 of 0.64−1.37 V s/cm^2, covering the diagonal scan line for doubly and triply charged precursors in the m/z-ion mobility plane.

Raw data were searched library-free against a SwissProt human database (January 2021) using DIA-NN 1.8. Database search criteria included tryptic cleavages permitting two missed cleavages, static carbamidomethylation of cysteine, variable oxidation of methionine, and a precursor Q-value (FDR) cutoff of 0.01. The precursor quantification strategy used was 'Robust LC (high accuracy)' with RT-dependent cross-run normalization. Resulting data was filtered to only include proteins that had a minimum of 3 precursor counts in all replicates of the DMSO control. Protein abundances in each sample were normalized by total protein and those with missing values were imputed by random selection from a Gaussian distribution. Significant changes in protein abundance in each treatment relative to the DMSO control were determined by a two-sided moderated t-test using the limma package in R.

Antiproliferation Assay (EGFR Ba/F3 Cells)

Cells were seeded at the density of 500 cells/well for 384-well plates and cultured overnight. Compounds were added into the media using drug dispenser for 72 h treatment. Cell viability was determined by using CellTiter-Glo (Promega #G7571) according to the manufacturer's instructions, measuring luminescence using a plate-reader. Dose−response curves were generated using nonlinear regression curve fit in GraphPad Prism.

In Vitro Cellular Efficacy Studies

Apoptosis was evaluated using the FITC Annexin V Apoptosis Detection Kit I (BD Pharmingen, San Diego, CA). Cells (0.2 × 10$\hat{6}$ per well) were treated with inhibitors overnight in 96-well plates. At least 10,000 events were acquired using a BD LSRFortessa Flow Cytometer, and results were analyzed using FlowJo software. For WM patient LPCs (0.2 × 10$\hat{6}$ per well), apoptosis was assessed using Alexa Fluor 700 antihuman CD19 antibody (Clone: HIB19, BioLegend) in combination with FITC Annexin V Apoptosis Detection Kit I.

Cellular Target Protein Degradation DC_{50} and D_{max} Determination Assay

TMD8 cells were treated with the indicated compounds for 16 h and subsequently lysed in RIPA buffer. Degradation of BTK and HCK was evaluated by Western blot using primary antibodies against BTK (clone D3H5, Cell Signaling Technology), HCK (clone E1I7F, Cell Signaling Technology), and GAPDH (clone D16H11, Cell Signaling Technology) as a loading control. Band intensities were quantified by densitometry using ImageJ software. The half-maximal degradation concentration (DC_{50}) and maximal protein degradation (D_{max}) were determined by four-parameter nonlinear regression analysis in GraphPad Prism.

Signaling Studies

Immunoblotting for key signaling proteins was performed using antibodies specific to phospho-BTK (Y223; Abcam 68217), BTK (CST 8547s), phospho−NF−κB (CST 3033s), NF-κB (CST 8242s), phospho-p44/p22 Mitogen-activated protein kinase (phosphor-ERK1/2; CST 4370s), ERK1/2 (CST 4696s), phospho-LYN (Tyr396) antibody (MA5−35882 from invitrogen and LYN cat# 2732 from Cell Signaling. Glyceraldehyde-3-phosphate dehydrogenase antibody (Santa Cruz 47724) was used as a loading control for the Western blots. DMSO (CAS: 67-68-5) was used as a vehicle control. For degradation rescue experiments, bortezomib, MLN4924 and ZXH-04−130 were purchased from MedChem Express.

In Vivo Efficacy Studies

To evaluate in vivo efficacy, MYD88^{Mut} TMD8 cells were xenografted into immunodeficient mice. Female NOD.Cg-Prkdc^{scid} Il2rg^{tm1Wjl}/SzJ (NSG) mice (7−8 weeks old) were obtained from The Jackson Laboratory (Bar Harbor, ME). All animal studies were conducted under IACUC-approved protocols at the Dana-Farber Cancer Institute. A total of 5 × 10^6 TMD8 cells were subcutaneously implanted with 1:1 Matrigel (Corning Life Sciences, Tewksbury, MA). Mice were randomly assigned to treatment cohorts when the average tumor volumes in the PD cohorts reached ∼400 mm^3 or 99.5 mm^3 in the efficacy cohort. Mice were treated once daily with either vehicle alone (10% 2-hydroxypropyl-β-cyclodextrin in water), DFCI-002-6, or KIN-8194by oral gavage (n = 9/group in efficacy study). Tumor volumes were measured twice weekly and calculated as (length × width^2 × 0.5).

Molecular Modeling

Molecular modeling was performed using the Molecular Operating Environment (MOE), version 2022.02 (Chemical Computing Group ULC, Montreal, QC, Canada). The X-ray crystal structures of HCK (PDB ID: 5ZJ6) and cereblon (PDB ID: 5FQD) were used for docking studies. Proteins were prepared by removing water molecules, adding hydrogens, and energy-minimizing prior to docking. Ligand structures were built in MOE and minimized using the MMFF94x force field prior to docking.

Statistical Analysis

Statistical significance was determined using one-way analysis of variance (ANOVA) with Tukey's multiple comparisons test (GraphPad Prism). Differences were considered statistically significant at $P < 0.05$. Error bars represent the standard error of the mean (SEM). Tumor volume comparisons were analyzed using the Dunn's multiple comparisons test.

Patient Samples

Mononuclear cells were isolated from bone marrow (BM) aspirates of diagnosed WM patients using Ficoll−Paque PLUS Media (GE Healthcare). BM mononuclear cells (0.2 × 10$\hat{6}$) were treated 20 h with vehicle control (DMSO), 0.5 μM of zanubrutinib, KIN-8194, or DFCI-002-6. Apoptosis was measured by flow cytometry using Annexin V-FITC and propidium iodide (PI) staining in the Alexa Fluor 700-CD19$^-$ and CD19$^+$ lymphoplasmacytic cells (LPCs). Clinical characteristics of the patients, including sex, age, MYD88 and CXCR4 mutation status, treatment history, drug resistance, IgM/IgG levels, and light chain status, are detailed in Table 1. Sample use was approved by the Dana-Farber/Harvard Cancer Center Institutional Review Board, and all patients provided written informed consent.

■ ASSOCIATED CONTENT

Supporting Information

The Supporting Information is available free of charge at https://pubs.acs.org/doi/10.1021/acs.jmedchem.5c02444.

Experimental procedures and analytical data for all synthetic intermediates and final compounds; full LC−MS and ^{1}H NMR spectra; detailed synthetic schemes; pharmacokinetic data in mice, rats, dogs, and hamsters; efficacy data in TMD8 xenograft models; comprehensive safety data including hERG inhibition, Ames mutagenicity. Kinome selectivity profiling of DFCI-002-06, DFCI-002-05, and Kin-8194; Western blot densitometry and degradation quantification (DC_{50} and Dmax values); patient clinical characteristics; and ADME characterization including CYP inhibition, Caco-2 permeability, hepatocyte and microsomal stability, and plasma protein binding (PDF)

21 day rat toxicology study (XLSX)

https://doi.org/10.1021/acs.jmedchem.5c02444
J. Med. Chem. 2026, 69, 1119−1134

Molecular Formula Strings (CSV)

AUTHOR INFORMATION

Corresponding Author

Steven P. Treon − *Bing Center for Waldenströms Macroglobulinemia, Dana-Farber Cancer Institute, Boston, Massachusetts 02215, United States; Department of Medicine, Harvard Medical School, Boston, Massachusetts 02115, United States*; Phone: (617) 632-2681; Email: steven_treon@dfci.harvard.edu; Fax: (617) 632-4862

Authors

John M. Hatcher − *Bing Center for Waldenströms Macroglobulinemia, Dana-Farber Cancer Institute, Boston, Massachusetts 02215, United States; Department of Medicine, Harvard Medical School, Boston, Massachusetts 02115, United States*; orcid.org/0000-0002-3540-7842

Shirong Liu − *Bing Center for Waldenströms Macroglobulinemia, Dana-Farber Cancer Institute, Boston, Massachusetts 02215, United States; Department of Medicine, Harvard Medical School, Boston, Massachusetts 02115, United States*

Amanda Kofides − *Bing Center for Waldenströms Macroglobulinemia, Dana-Farber Cancer Institute, Boston, Massachusetts 02215, United States*

Alexa Canning − *Bing Center for Waldenströms Macroglobulinemia, Dana-Farber Cancer Institute, Boston, Massachusetts 02215, United States*

Dominic Pizzarella − *Bing Center for Waldenströms Macroglobulinemia, Dana-Farber Cancer Institute, Boston, Massachusetts 02215, United States*

Xia Liu − *Bing Center for Waldenströms Macroglobulinemia, Dana-Farber Cancer Institute, Boston, Massachusetts 02215, United States*

Nickolas Tsakmaklis − *Bing Center for Waldenströms Macroglobulinemia, Dana-Farber Cancer Institute, Boston, Massachusetts 02215, United States*

Maria Guerrera − *Bing Center for Waldenströms Macroglobulinemia, Dana-Farber Cancer Institute, Boston, Massachusetts 02215, United States; Department of Medicine, Harvard Medical School, Boston, Massachusetts 02115, United States*

Christopher Patterson − *Bing Center for Waldenströms Macroglobulinemia, Dana-Farber Cancer Institute, Boston, Massachusetts 02215, United States*

Alberto Guijosa − *Bing Center for Waldenströms Macroglobulinemia, Dana-Farber Cancer Institute, Boston, Massachusetts 02215, United States; Department of Medicine, Harvard Medical School, Boston, Massachusetts 02115, United States*

Prafulla Gokhale − *Experimental Therapeutics Core and Belfer Center for Applied Cancer Science, Dana-Farber Cancer Institute, Boston, Massachusetts 02215, United States*

Zachary Hunter − *Bing Center for Waldenströms Macroglobulinemia, Dana-Farber Cancer Institute, Boston, Massachusetts 02215, United States; Department of Medicine, Harvard Medical School, Boston, Massachusetts 02115, United States*

Shayna Sarosiek − *Bing Center for Waldenströms Macroglobulinemia, Dana-Farber Cancer Institute, Boston, Massachusetts 02215, United States; Department of Medicine, Harvard Medical School, Boston, Massachusetts 02115, United States*

Jorge Castillo − *Bing Center for Waldenströms Macroglobulinemia, Dana-Farber Cancer Institute, Boston, Massachusetts 02215, United States; Department of Medicine, Harvard Medical School, Boston, Massachusetts 02115, United States*

Jinhua Wang − *Department of Cancer Biology, Harvard Medical School, Dana-Farber Cancer Institute; Department of Biological Chemistry and Molecular Pharmacology, Boston, Massachusetts 02115, United States*

Sara J. Buhrlage − *Department of Cancer Biology, Harvard Medical School, Dana-Farber Cancer Institute; Department of Biological Chemistry and Molecular Pharmacology, Boston, Massachusetts 02115, United States*; orcid.org/0000-0003-4562-1823

Complete contact information is available at: https://pubs.acs.org/10.1021/acs.jmedchem.5c02444

Author Contributions

[⊥]J.M.H. and S.L. contributed equally to this work. The manuscript was written through contributions of all authors. All authors have given approval to the final version of the manuscript.

Funding

The authors gratefully acknowledge the generous support of the Leukemia and Lymphoma Society (Grant: 6673-24), the International Waldenstrom's Macroglobulinemia Foundation, the Siegel Family Fund for WM, the Kerry Robertson Fund for WM Research, the Lee and Michael Bell WM Fellowship (SL), the Jan Gosta Waldenstrom Fellowship for Therapeutic Advancements (JMH), and the Forstall Fund for Next-Generation WM Therapies

Notes

The authors declare the following competing financial interest(s): SPT received research funding, and/or consulting fees from Abbvie/Pharmacyclics Inc., Janssen Oncology Inc., Beigene Inc., Eli Lilly Pharmaceuticals, Bristol Myers Squibb, and Ono Pharmaceuticals. JJC received research funds or consulting fees from Abbvie, AstraZeneca, Avilar, BeOne, Cellectar, Johnson & Johnson, LOXO, and Pharmacyclics. SRS received research funding and/or consulting fees from ADC Therapeutics, Beigene, Cellectar, and SOBI. JW is a consultant and equity holder at Soltego. All other authors declare no conflicts of interest.

Ethics Statement: All animal experiments performed at the Dana-Farber Cancer Institute were conducted following protocols evaluated and approved by the Dana-Farber Cancer Institute Institutional Animal Care and Use Committee (IACUC Protocol Number: 04-111). Rat toxicity studies performed at The Scripps Research Institute, Florida Campus, were conducted in accordance with protocols approved by the Scripps Research Institute Institutional Animal Care and Use Committee (IACUC Protocol Number: 17-008-03). Pharmacokinetic studies conducted at ChemPartner were performed in AAALAC-accredited facilities and in compliance with institutional guidelines and all applicable national regulations. All procedures complied with the National Institutes of Health Guide for the Care and Use of Laboratory Animals.

https://doi.org/10.1021/acs.jmedchem.5c02444
J. Med. Chem. 2026, 69, 1119−1134

■ ACKNOWLEDGMENTS

The authors wish to thank Choudhury Fabliha B. Yusuf for help with the in vivo studies.

■ REFERENCES

(1) Treon, S. P.; Xu, L.; Yang, G.; Zhou, Y.; Liu, X.; Cao, Y.; Sheehy, P.; Manning, R. J.; Patterson, C. J.; Tripsas, C.; et al. MYD88 L265P somatic mutation in Waldenstrom's macroglobulinemia. *N. Engl. J. Med.* **2012**, *367* (9), 826−833.

(2) Xu, L.; Hunter, Z. R.; Yang, G.; Zhou, Y.; Cao, Y.; Liu, X.; Morra, E.; Trojani, A.; Greco, A.; Arcaini, L.; et al. MYD88 L265P in Waldenstrom macroglobulinemia, immunoglobulin M monoclonal gammopathy, and other B-cell lymphoproliferative disorders using conventional and quantitative allele-specific polymerase chain reaction. *Blood* **2013**, *121* (11), 2051−2058.

(3) Nakamura, T.; Tateishi, K.; Niwa, T.; Matsushita, Y.; Tamura, K.; Kinoshita, M.; Tanaka, K.; Fukushima, S.; Takami, H.; Arita, H.; et al. Recurrent mutations of CD79B and MYD88 are the hallmark of primary central nervous system lymphomas. *Neuropathol. Appl. Neurobiol.* **2016**, *42* (3), 279−290.

(4) Ngo, V. N.; Young, R. M.; Schmitz, R.; Jhavar, S.; Xiao, W.; Lim, K. H.; Kohlhammer, H.; Xu, W.; Yang, Y.; Zhao, H.; et al. Oncogenically active MYD88 mutations in human lymphoma. *Nature* **2011**, *470* (7332), 115−119.

(5) Martinez-Lopez, A.; Curiel-Olmo, S.; Mollejo, M.; Cereceda, L.; Martinez, N.; Montes-Moreno, S.; Almaraz, C.; Revert, J. B.; Piris, M. A. MYD88 (L265P) somatic mutation in marginal zone B-cell lymphoma. *Am. J. Surg Pathol* **2015**, *39* (5), 644−651.

(6) Landau, D. A.; Carter, S. L.; Stojanov, P.; McKenna, A.; Stevenson, K.; Lawrence, M. S.; Sougnez, C.; Stewart, C.; Sivachenko, A.; Wang, L.; et al. Evolution and impact of subclonal mutations in chronic lymphocytic leukemia. *Cell* **2013**, *152* (4), 714−726.

(7) Yang, G.; Zhou, Y.; Liu, X.; Xu, L.; Cao, Y.; Manning, R. J.; Patterson, C. J.; Buhrlage, S. J.; Gray, N.; Tai, Y. T.; et al. A mutation in MYD88 (L265P) supports the survival of lymphoplasmacytic cells by activation of Bruton tyrosine kinase in Waldenstrom macroglobulinemia. *Blood* **2013**, *122* (7), 1222−1232.

(8) Yang, G.; Buhrlage, S. J.; Tan, L.; Liu, X.; Chen, J.; Xu, L.; Tsakmaklis, N.; Chen, J. G.; Patterson, C. J.; Brown, J. R.; et al. HCK is a survival determinant transactivated by mutated MYD88, and a direct target of ibrutinib. *Blood* **2016**, *127* (25), 3237−3252.

(9) Liu, X.; Chen, J. G.; Munshi, M.; Hunter, Z. R.; Xu, L.; Kofides, A.; Tsakmaklis, N.; Demos, M. G.; Guerrera, M. L.; Chan, G. G.; et al. Expression of the prosurvival kinase HCK requires PAX5 and mutated MYD88 signaling in MYD88-driven B-cell lymphomas. *Blood Adv.* **2020**, *4* (1), 141−153.

(10) Munshi, M.; Liu, X.; Chen, J. G.; Xu, L.; Tsakmaklis, N.; Demos, M. G.; Kofides, A.; Guerrera, M. L.; Jimenez, C.; Chan, G. G.; et al. SYK is activated by mutated MYD88 and drives pro-survival signaling in MYD88 driven B-cell lymphomas. *Blood Cancer J.* **2020**, *10* (1), 12.

(11) Munshi, M.; Liu, X.; Kofides, A.; Tsakmaklis, N.; Guerrera, M. L.; Hunter, Z. R.; Palomba, M. L.; Argyropoulos, K. V.; Patterson, C. J.; Canning, A. G.; et al. A new role for the SRC family kinase HCK as a driver of SYK activation in MYD88 mutated lymphomas. *Blood Adv.* **2022**, *6* (11), 3332−3338.

(12) Treon, S. P.; Sarosiek, S.; Castillo, J. J. How I use genomics and BTK inhibitors in the treatment of Waldenstrom macroglobulinemia. *Blood* **2024**, *143* (17), 1702−1712.

(13) Xu, L.; Tsakmaklis, N.; Yang, G.; Chen, J. G.; Liu, X.; Demos, M.; Kofides, A.; Patterson, C. J.; Meid, K.; Gustine, J.; et al. Acquired mutations associated with ibrutinib resistance in Waldenstrom macroglobulinemia. *Blood* **2017**, *129* (18), 2519−2525.

(14) Taguchi, T.; Kiyokawa, N.; Sato, N.; Saito, M.; Fujimoto, J. Characteristic expression of Hck in human B-cell precursors. *Exp Hematol* **2000**, *28* (1), 55−64.

(15) Gutierrez, N. C.; Ocio, E. M.; de Las Rivas, J.; Maiso, P.; Delgado, M.; Ferminan, E.; Arcos, M. J.; Sanchez, M. L.; Hernandez, J. M.; San Miguel, J. F. Gene expression profiling of B lymphocytes and plasma cells from Waldenstrom's macroglobulinemia: comparison with expression patterns of the same cell counterparts from chronic lymphocytic leukemia, multiple myeloma and normal individuals. *Leukemia* **2007**, *21* (3), 541−549.

(16) Chen, J. G.; Liu, X.; Munshi, M.; Xu, L.; Tsakmaklis, N.; Demos, M. G.; Kofides, A.; Guerrera, M. L.; Chan, G. G.; Patterson, C. J.; et al. BTK(Cys481Ser) drives ibrutinib resistance via ERK1/2 and protects BTK(wild-type) MYD88-mutated cells by a paracrine mechanism. *Blood* **2018**, *131* (18), 2047−2059.

(17) Tam, C. S.; Balendran, S.; Blombery, P. Novel mechanisms of resistance in CLL: variant BTK mutations in second-generation and noncovalent BTK inhibitors. *Blood* **2025**, *145* (10), 1005−1009.

(18) Dhami, K.; Chakraborty, A.; Gururaja, T. L.; Cheung, L. W.; Sun, C.; DeAnda, F.; Huang, X. Kinase-deficient BTK mutants confer ibrutinib resistance through activation of the kinase HCK. *Sci. Signal* **2022**, *15* (736), No. eabg5216.

(19) Seymour, J.; Tam, C. S.; Cheah, C. Y.; Parrondo, R. D.; Allan, J. N.; Trotman, J.; Advani, R. H.; Eradat, H. A.; Zinzani, P. L.; Lasica, M.; et al. Preliminary Efficacy and Safety of the Bruton Tyrosine Kinase Degrader BGB-16673 in Patients with Relapsed or Refractory Waldenström Macroglobulinemia: Results from the Phase 1 CaDAnCe-101 Study. *Blood* **2024**, *144* (Supplement 1), 860.

(20) El-Sharkawi, D.; Lewis, D.; Pulles, A.; et al. *Bexobrutideg (NX-5948), a novel Bruton's Tyrosine Kinase Degrader, shows high clinical activity and tolerable safety in an ongoing Phase 1A/B study in patients with Waldenström Macroglobulinemia*. In *Proceedings of the European Hematology Association*, 2025.

(21) Wong, R. L.; Choi, M. Y.; Wang, H. Y.; Kipps, T. J. Mutation in Bruton Tyrosine Kinase (BTK) A428D confers resistance To BTK-degrader therapy in chronic lymphocytic leukemia. *Leukemia* **2024**, *38* (8), 1818−1821.

(22) Yang, G.; Wang, J.; Tan, L.; Munshi, M.; Liu, X.; Kofides, A.; Chen, J. G.; Tsakmaklis, N.; Demos, M. G.; Guerrera, M. L.; et al. The HCK/BTK inhibitor KIN-8194 is active in MYD88-driven lymphomas and overcomes mutated BTKCys481 ibrutinib resistance. *Blood* **2021**, *138* (20), 1966−1979.

(23) Sievers, Q. L.; Petzold, G.; Bunker, R. D.; Renneville, A.; Słabicki, M.; Liddicoat, B. J.; Abdulrahman, W.; Mikkelsen, T.; Ebert, B. L.; Thoma, N. H. Defining the human C2H2 zinc finger degrome targeted by thalidomide analogs through CRBN. *Science* **2018**, *362* (6414), No. eaat0572.

(24) Bricelj, A.; Dora Ng, Y. L.; Ferber, D.; Kuchta, R.; Muller, S.; Monschke, M.; Wagner, K. G.; Kronke, J.; Sosic, I.; Gutschow, M.; et al. Influence of Linker Attachment Points on the Stability and Neosubstrate Degradation of Cereblon Ligands. *ACS Med. Chem. Lett.* **2021**, *12* (11), 1733−1738.

(25) Sathe, G.; Sapkota, G. P. Proteomic approaches advancing targeted protein degradation. *Trends Pharmacol. Sci.* **2023**, *44* (11), 786−801.

(26) Mostofian, B.; Martin, H. J.; Razavi, A.; Patel, S.; Allen, B.; Sherman, W.; Izaguirre, J. A. Targeted Protein Degradation: Advances, Challenges, and Prospects for Computational Methods. *J. Chem. Inf. Model.* **2023**, *63* (17), 5408−5432.

(27) Powell, C. E.; Du, G.; Bushman, J. W.; He, Z.; Zhang, T.; Fischer, E. S.; Gray, N. S. Selective degradation-inducing probes for studying cereblon (CRBN) biology. *RSC Med. Chem.* **2021**, *12* (8), 1381−1390.

(28) Hornberger, K. R.; Araujo, E. M. V. Physicochemical Property Determinants of Oral Absorption for PROTAC Protein Degraders. *J. Med. Chem.* **2023**, *66* (12), 8281−8287.

(29) Liu, S.; Liu, X.; Kofides, A.; Hatcher, J.; Tsakmaklis, N.; Peachey, A.; Pizzarella, D.; Guijosa, A.; Wang, J.; Guerrera, M. L.; et al. Diverse signaling and vulnerabilities accompany distinct BTK mutations associated with clinical resistance to covalent, non-covalent and PROTACs targeting BTK in MYD88 mutated lymphomas. *Blood* **2025**, *146*, 2171.

(30) Sun, H.; Sklavenitis-Pistofidis, R.; Liu, X.; Tsakmaklis, N.; Guerrera, M. L.; Kofides, A.; Gamero, A. F. R.; Flynn, C. A.; Patterson, C. J.; Hao, M.; et al. Genomic evolution by serial single-cell sequencing identifies high tumor expression of LYN as a promoter of resistance in

https://doi.org/10.1021/acs.jmedchem.5c02444
J. Med. Chem. 2026, 69, 1119−1134

Waldenstrom's Macroglobulinemia undergoing ibrutinib monotherapy. *Blood* **2024**, *144* (Supplement 1), 4338.

https://doi.org/10.1021/acs.jmedchem.5c02444
J. Med. Chem. 2026, 69, 1119−1134